Mechanically Interlocked Resilient Additives (MIRA)

Final Report

Payable Milestone #8: Large (0.5 kg) scale synthesis of high-quality polymer-COF composites with enhanced mechanical properties.

Contract/Agreement Number: HR00112290097

Submission Date: 01/14/2024

Resubmission Date: 02/16/2024

Recipient Organization: The Regents of the University of California Berkeley, 602 Latimer Hall, UC Berkeley, CA 94720-7635

PI Point of Contact: Omar M. Yaghi

TABLE OF CONTENTS

1. Executive Summary

Throughout the performance period of this project, teams from UC Berkeley, GE Research, and the University of Southern Alabama (USA) developed strategies to synthesize and characterize a new class of polymer composites. Based upon the principles of molecularly interlocked molecules (MIMs), the teams generated woven and interlocked covalent organic frameworks (COFs) to be used as filler materials in different polymer systems. The resulting composites were tested for enhanced performance and the filler-matrix interactions were characterized by a variety of techniques.

UC Berkeley reported meaningful advancements in the synthesis, characterization, and scaling of metal-free woven and interlocked COFs. Initial target structures were tested for their scalability, which also included an investigation into the accessibility of starting materials. Specifically, methodologies to scale woven COF-506 both by reflux and solvothermal syntheses were developed to reach multi-gram scale. The recycling of metal ions from the demetallation process was achieved via a chemical reduction of copper ions. These studies resulted in two pathways to produce and demetalate imine-linked and amine-linked woven COFs. These findings are directly translatable to other COFs, which poses significant progress in the feasibility of this class of materials. Furthermore, the Berkeley team employed characterization techniques involving 2D solid-state nuclear magnetic resonance (NMR) techniques provided valuable insight into the polymer-COF interactions in the composites. These studies revealed two types of possible interactions between the polymer matrix and the framework fillers. Polymethylmethacrylate (PMMA) showed surface interactions with the woven COFs, which resulted in marginal or no improvements in the mechanical behavior of the resulting composites. However, the interactions of the COF with polyimide (PI) revealed significant spatial closeness between the polymer backbone and the framework. This was rationalized with a threading of the polymer strands into the pore structures, which correlated with more promising mechanical enhancement. Further understanding of parameters such as chemical composition and molecular weight are required to elucidate the complex polymer-COF systems.

During this period GE Research demonstrated significant improvements in synthetic methodology, mechanical test methodologies, and materials characterization. The primary goals of our work were to screen new polymer-COF composite systems, provide a path toward larger scale synthesis, demonstrate material performance enhancement, and use materials characterization to support optimization and deepen understanding of the composite system. The early phases of the program were dedicated to demonstrating analytical capability and reproducing prior results. Once capability was established COF-polymer composites with polyimide (PI), acrylonitrile-butadiene-styrene (ABS), polymethylmethacrylate (PMMA), polycarbonate (PC), polydimethylsiloxane (PDMS), chitosan, epoxy, and polystyrene (PS) were prepared and evaluated for mechanical properties. Of the materials evaluated polycarbonate (PC) and polydimethylsiloxane (PDMS), both with COF 506-imine, yielded the most satisfactory results. On final scale-up, a 200-gram scale silicone-COF composite demonstrated a significant

improvement in properties doubling the tensile strength from 8 to 17 MPa and increasing the elongation from 181% to 225%. A 100-gram final scale-up of polycarbonate composite showed an increase in strength from 45 to 64 MPa with a drop in strain from 74% to 24%. End-group analysis by NMR and rheologic methods were developed for analyzing the polyimide precursors and solutions allowing synthetic optimization and were able to be correlated to the tensile strength of cured polymer films.

Systematic studies aimed at investigating the surface properties, mechanical behaviors, and nanoparticle interactions within polymer films and nanocomposites were performed. The surface characteristics of polycarbonate (PC) and polydimethylsiloxane (PDMS) films were examined under varied treatment durations and loadings of covalent organic framework (COF). The analysis involved parameters such as surface roughness, contact angles, and surface free energy components. The mechanical properties of the films were explored the tensile strength of the composite films were found to be well correlated to the surface free energy. Microstructure analysis provided insights into the relationship between area roughness parameters and strength parameters. Solution viscosity and surface free energy investigations explored the impact of nanoparticles on polymer relaxation, revealing a unique slowing effect across different timescales and particle concentrations. This study emphasized the formation and stability of the interphase in polymer-nanoparticle composites (PNCs). The interphase, influenced by factors like nanoparticle size, surface chemistry, and polymer-nanoparticle interactions, significantly influenced the overall material properties. A stable interphase ensured uniform nanoparticle dispersion and optimal interfacial adhesion, enhancing the composite's mechanical performance. Johnson–Kendall–Roberts (JKR) theory was applied to understand nanoparticle contact mechanics. Discrepancies between theoretical predictions and experimental data were attributed to factors like adhesive forces, surface roughness, non-elastic behavior, size-dependent effects, and nuanced experimental conditions at the nanoscale.

The USA team examined the diffusion of gases into COFs, metalated COFs, and woven COF materials to determine if diffusion rate, mechanism, or isotherm shape could be used to identify the presence of molecular scale weaving. At the start of the project, very little data existed on the adsorption of gases into COF materials, but upon conclusion of this effort, details about which gases adsorbed in COFs with and without metals, and how the gases diffuse through the materials have been established. The results showed that although COFs are comprised primarily of porous carbon, the adsorption dynamics of these materials are not analogous to simpler materials such as activated carbon. The materials, generally, exhibited unique adsorption selectivity for polar materials over non-polar materials and fast gas phase diffusion dynamics. Seven different adsorbates were examined for both adsorption capacity and diffusion rate across 4 different adsorbent materials. The diffusion measurements seem to indicate that tetrahydrofuran does diffuse into a COF-PI woven sample via two distinct pore openings. To describe this behavior, a parallel pore diffusion model was developed that is consistent with a woven pore and a non-woven pore each contributing to the total adsorption loading. Surprisingly, not all adsorbates show this

behavior. More experiments are needed to determine how reproducible the parallel pore results are and over what types of adsorbates this behavior is observed. More broadly, the adsorption data highlight that COF materials are complex, the behaviors are unique, and more research effort should be applied to understand the behaviors of these materials more fully.

In summary, this work demonstrated that covalent organic frameworks could act as reinforcing agents in select polymers and elastomers. The exploration of the behaviors of the COFs within polymer films and nanocomposites demonstrated interactions that might be exploited to further enhance the reinforcing effects of the COF nanoparticles. Furthermore, COFs were found to be chemically active, suppressing polymerization of PMMA and PS by radical mechanisms. This suggests that COFs need to be tailored to be neutral to certain polymerizations methods but also might be modified to participate synergistically with other systems. The findings presented herein contribute to a deeper understanding of the complex dynamics involved, offering valuable insights for material design and optimization in various applications. As the findings from the preceding grant on polymer-COF composites have resulted in the publication of high-impact manuscripts,[1-3] the work performed in this project has contributed to and will result in further publications that will likely shape a path for future investigations.

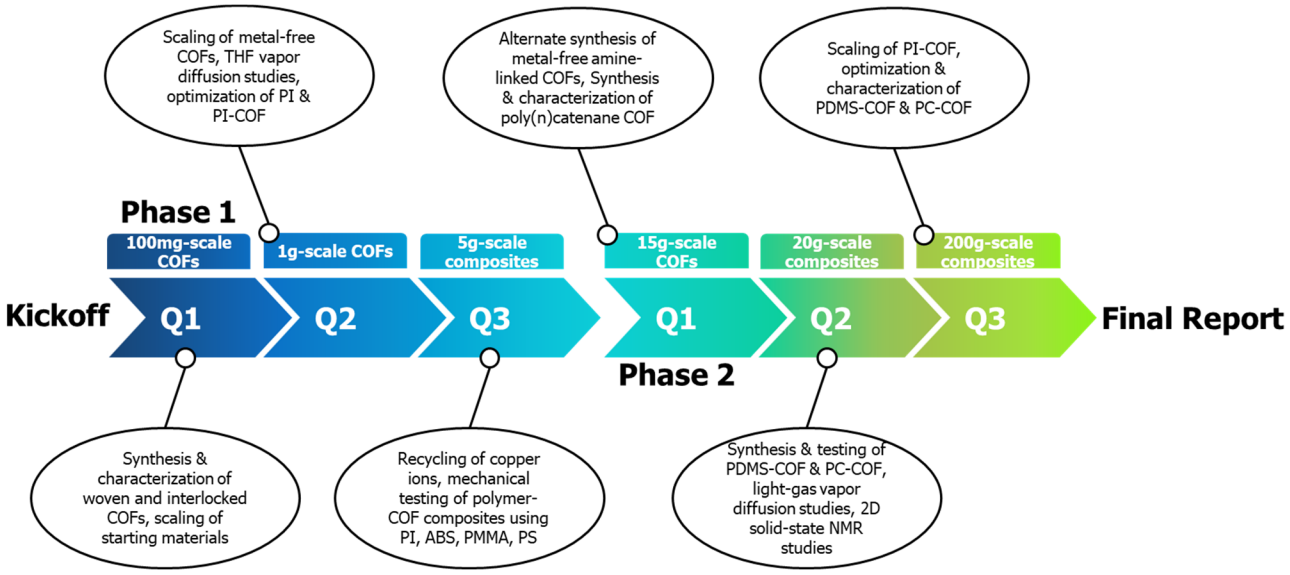

2. Woven & Interlocked Covalent Organic Frameworks

2.1 Large-Scale Synthesis of Woven and Interlocked COFs

To employ woven and interlocked COFs as mechanically interlocked resilient additives (MIRAs) in the synthesis of polymer composites, the team improved the scalability of the COFs with an overall metal-free synthetic strategy. The progress toward reaching intermediate synthetic scalability (multi-gram scale), demetalation, and recovery of metals used in the synthesis of the COFs is detailed in this section.

2.1.1 Theoretical design and synthesis of woven and interlocked COFs

The synthetic design of covalent organic frameworks (COFs) is based on the principles of Reticular Chemistry. Generally, COFs are constructed from one or more building units that are linked through covalent bonds. The reversibility of linkages, such as the formation of imines, offers a pathway for error correction during the construction of the porous framework structures. This allows for the synthesis of highly crystalline COFs (Figure 1).[4]

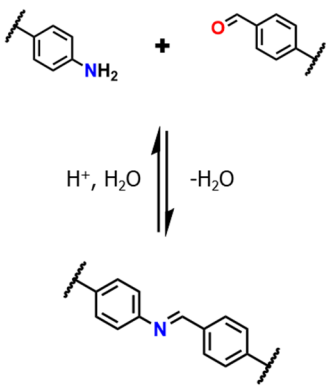

Figure 1. Reversible imine bond formation allows for highly crystalline COFs.

To achieve woven or interlocked COF structures, we implement metal-organic weaving nodes, which have previously been employed in the synthesis of mechanically interlocked molecules (MIMs), such as catenanes and rotaxanes.[5] Specifically, we make use of a complex formed by Cu(I) salts and aldehyde-functionalized phenanthroline molecules. This results in the formation of a tetrahedral weaving node that can be combined with amine-functionalized linkers baring different geometries to give varying woven and interlocked frameworks. The structures that we target in this effort can be classified as woven, interlocked, braided, and interlocked cages (Figure 2). The need for careful selection of staring materials is highlighted in the woven COFs-505 and 506 as well as the interlocked COF-500. For example, the use of a copper phenanthroline complex with BF_4^- anions leads to the generation of an interpenetrated woven structure, reported as COF-505.[6] In contrast, changing the counter anion to $PO_2Ph_2^-$, which is comparatively large, results in the synthesis of the woven, non-interpenetrated woven COF-506.[7] Additionally, a different geometry in the amine linker (planar instead of linear) not only changes the structure of the received COF from woven to interlocked, but also has a dramatic impact on the optimized reaction conditions.[8] Optimized reaction conditions for all proposed COFs are detailed in Table 1, which include specific temperature, solvent system, amount of acid catalyst, and reaction time. The reactions were optimized on a 1-mL scale (reaction volume).

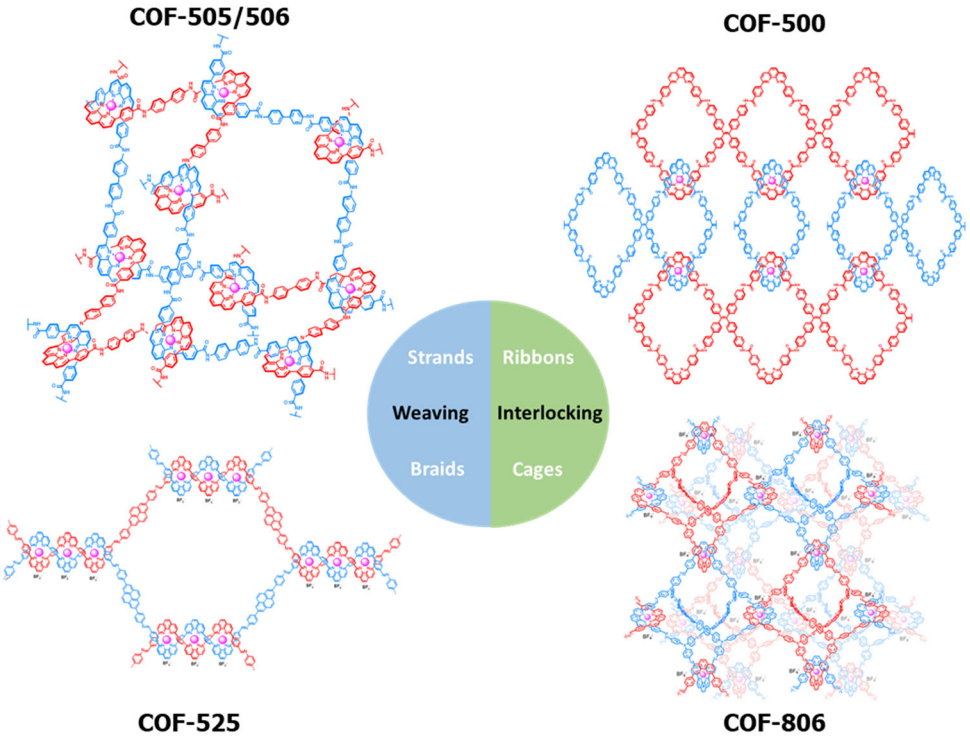

Figure 2. Targeted woven and interlocked frameworks.[1, 2, 6-9] The woven COFs-505 and 506 are constructed from 1D organic threads that result from the combination of tetrahedral weaving nodes with a linear linker (benzidine). Interlocked COF-500 is formed by 1D square ribbons that interlock into a 3D framework pattern. COF-525 exhibits a new type of molecular weaving, braiding, that is inspired by helicate structures to generate a 2D COF. Combining a trigonal amine linker with the tetrahedral weaving node results in the formation of COF-806, which is easiest compared to interlocked cages within a 3D framework.

Table 1. Optimized reaction conditions for woven and interlocked COFs.

	Temperature / °C	**Solvent system**	**Acid catalyst**	**Reaction time / h**
COF-500	180	Dichlorobenzene/ 1-butanol (1:1)	Acetic acid (0.1 mL, 9M)	72
COF-506	120	1,4-dioxane/ Mesitylene (7:3)	Acetic acid 0.1 mL, 6M)	72
COF-525	120	Chlorobenzene/ Dimethylacetamide (6:4)	Acetic acid (0.15 mL, 6M)	72
COF-806	120	1,4-dioxane	Acetic acid (0.2 mL, 6M)	72

2.1.2 Analysis and characterization of woven and interlocked COFs

The data discussed in the following is presented in the following figures 3 - 6. To ensure the formation of the respective woven and interlocked framework structures, the COFs are

characterized by powder X-ray diffraction (PXRD). The patterns are matched to computational models of the structures. In addition, Fourier-transform infrared (FTIR) spectroscopy is employed to confirm the formation of imine linkages. The appearance of characteristic imine bond (C=N) stretches is observed at wavenumber ranges of 1628 cm^{-1} to 1650 cm^{-1}. At the same time, the prominent aldehyde (C=O) stretch disappears, ranging from 1660 cm^{-1} to 1710 cm^{-1}. This evidence indicates the successful formation of imine-linked framework structures and, in combination with PXRD evidence, confirms the formation of the COFs.

Scanning electron microscopy (SEM) is used to monitor the homogeneity, morphology, and size of the COF crystallites. Generally, the COF crystals range from 300 nm to a few microns in size and show homogenous morphologies for every material proposed in this effort. Additionally, thermogravimetric analysis (TGA) provides important information about the thermal stability of the COFs. Every woven or interlocked COF exhibits good thermal stability ranging from 350 to 400 °C in an inert atmosphere, which allows the materials to be processed in a wide temperature range.

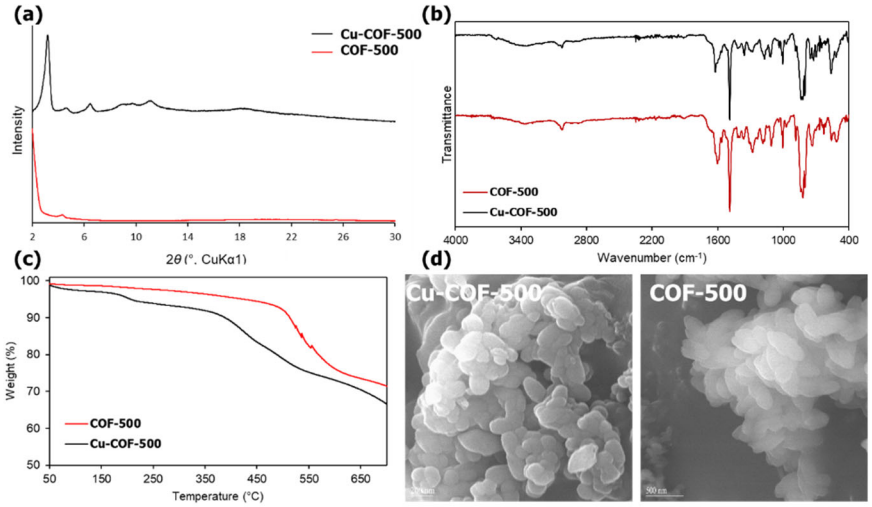

Figure 3. Characterization of interlocked COF-500 before and after demetalation. (a) PXRD spectra of metalated Cu-COF-500 and demetalated COF-500. Crystallinity is lost as expected after removal of the copper ions from the structure. **(b)** FTIR spectra of metalated Cu-COF-500 and demetalated COF-500. The characteristic imine bond stretch at 1628 cm^{-1} is observed in both frameworks. **(c)** TGA of metalated Cu-COF-500 and demetalated COF-500. Thermal stability is not impacted by the loss of copper ions. **(d)** SEM micrographs of metalated Cu-COF-500 and demetalated COF-500. The shape and size of the kernel-shaped crystallites, ranging from 300 – 400 nm, do not change throughout the processing.

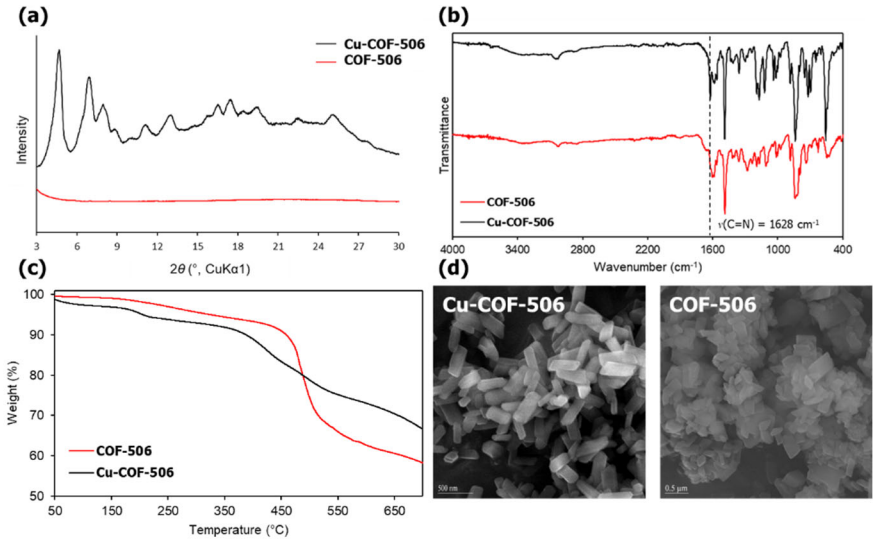

Figure 4. Characterization of interlocked COF-506 before and after demetalation. (a) PXRD spectra of metalated Cu-COF-506 and demetalated COF-506. Crystallinity is lost as expected after removal of the copper ions from the structure. **(b)** FTIR spectra of metalated Cu-COF-506 and demetalated COF-506. The characteristic imine bond stretch at 1628 cm^{-1} is observed in both frameworks. **(c)** TGA of metalated Cu-COF-506 and demetalated COF-506. Thermal stability is not impacted by the loss of copper ions. **(d)** SEM micrographs of metalated Cu-COF-506 and demetalated COF-506. The shape and size of the rod-shaped crystallites, ranging from 300 – 500 nm, do not change throughout the processing.

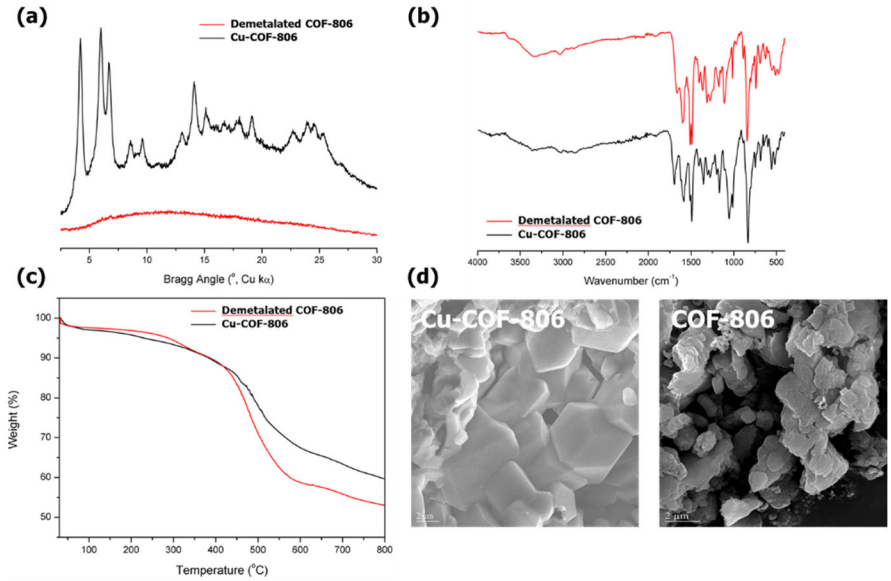

Figure 5. Characterization of interlocked COF-806 before and after demetalation. (a) PXRD spectra of metalated Cu-COF-806 and demetalated COF-806. Crystallinity is lost as expected after removal of the copper ions from the structure. **(b)** FTIR spectra of metalated Cu-COF-806 and demetalated COF-806. The characteristic imine bond stretch at 1636 cm^{-1} is observed in both frameworks. **(c)** TGA of metalated Cu-COF-806 and demetalated COF-806. Thermal stability is not impacted by the loss of copper ions. **(d)** SEM micrographs of metalated Cu-COF-806 and demetalated COF-806. The shape and size of the crystallites, ranging from 1 – 2 μm, do not change throughout the processing.

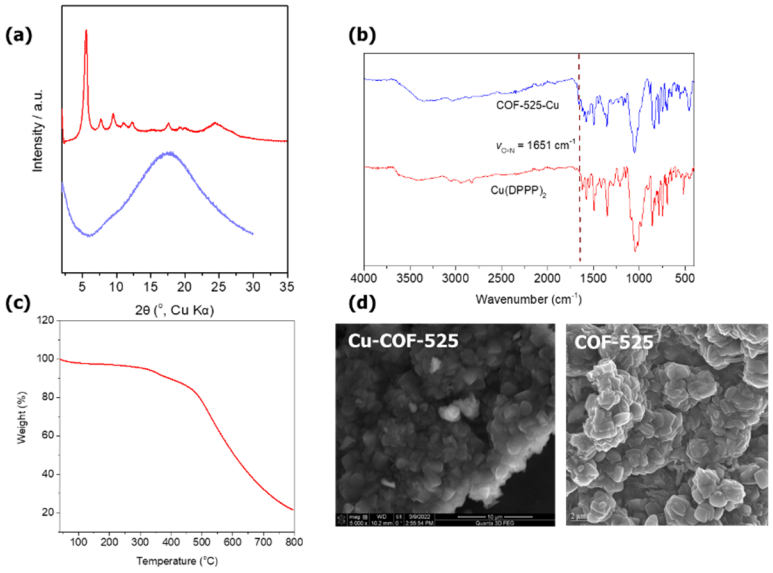

Figure 6. Characterization of interlocked COF-525 before and after demetalation. (a) PXRD spectra of metalated Cu-COF-525 and demetalated COF-525. Crystallinity is lost as expected after removal of the copper ions from the structure. **(b)** FTIR spectra of metalated Cu-COF-525 and demetalated COF-525. The characteristic imine bond stretch at 1632 cm^{-1} is observed in both frameworks. **(c)** TGA of metalated Cu-COF-525. **(d)** SEM micrographs of metalated Cu-COF-525 and demetalated COF-525. The shape and size of the kernel-shaped crystallites, ranging from 0.5 – 1 µm, do not change throughout the processing.

After the demetalation process, the crystallinity of the COFs is drastically reduced, which is attributed to the increased degrees of freedom after the removal of copper ions from the weaving nodes. The framework structures are held together solely through mechanical bonding, and the enhanced mobility of separate parts of the structure lead to the observed loss in long range order. Importantly, the FTIR spectra of the COFs before and after the removal of metal ions shows no change in the characteristic imine-bond stretch, thereby confirming the remaining linkages within the frameworks. The disappearance of anion-related signals (e.g., B-F stretch from BF_4^-) further supports the removal of the copper ions. Quantitative evidence for the complete removal of the copper ions from the structures is gained by inductively coupled plasma atomic emission spectroscopy (ICP-AES). Each of the woven and interlocked structures loses up to 99% of the copper ions within the structure. SEM and TGA characterization further support the maintained integrity of the COFs after the demetaltion process by showing no change in crystallite size and shape, as well as indicating no loss in thermal stability.

2.1.3 Synthetic Scalability of Woven and Interlocked COFs

To produce high-performance polymer composites containing MIMs, the UC Berkeley team worked to improve the scalability of the woven and interlocked COFs.[6-8] The progress in phase 1 is summarized in Table 2.

Table 2. Progress toward scalability of woven and interlocked COFs in phase 1.

	Synthesis & Characterization	Starting Material	Scaling Methods	Scale
COF-500	Completed	Scalable, commercial	Solvothermal, reflux	gram
COF-506	Completed	Scalable, commercial	Solvothermal	gram
COF-525	Completed	Difficult to scale	Solvothermal	milligram
COF-806	Completed	Scalable, commercial	Solvothermal	milligram

Initial testing into possible synthetic methods for COFs focused on the use of either solvothermal or microwave reactors. Whereas the woven COF-506 was readily scalable with either method, the interlocked COF-500 showed greatly diminished quality as evident by the PXRD patterns in figure 7. To overcome the limited scalability of COF-500, the team was able to increase the crystallinity of the product by increasing the reaction volume. Interestingly, the scaling of the synthesis of both COF-500 and COF-506 did not greatly affect the yield (70-82 % for COF-500, 75-80 % for COF-506) (Figure 8).

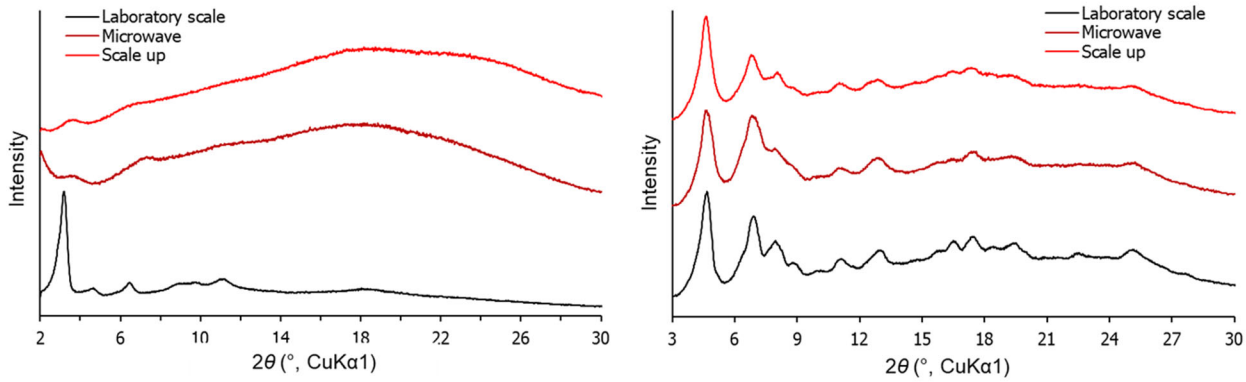

Figure 7. PXRD spectra of woven COF-506 and interlocked COF-500 synthesized in sealed glass tubes, microwave reactors, or pressure tubes. (left) Comparison of the PXRD spectra of the interlocked COF-500 synthesized in different reaction vessels shows that the scaled-up products or not crystalline. **(right)** Comparison of the PXRD spectra of COF-506 synthesized in different reaction vessels shows highly crystalline products scaled up in both the microwave reactor and the pressure tube.

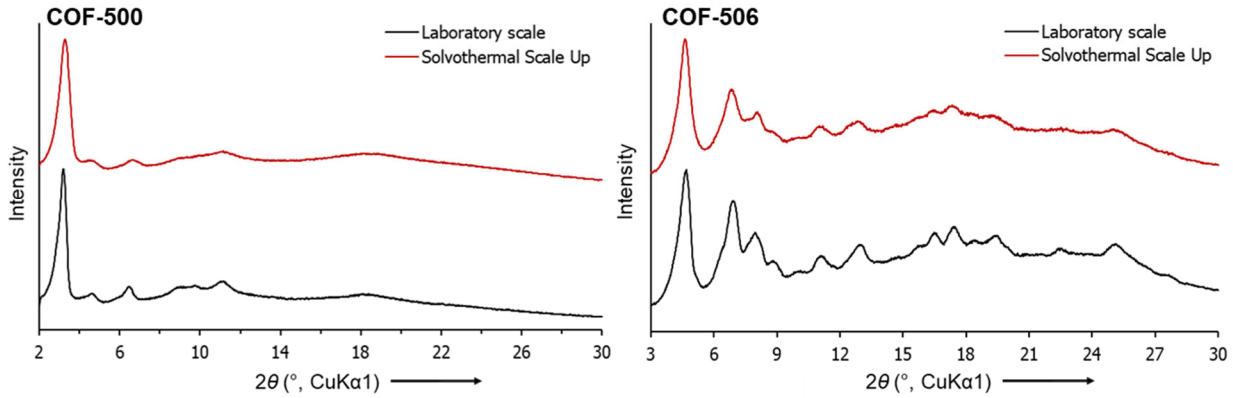

Figure 8. PXRD patterns of interlocked COF-500 (left) and woven COF-506 (right). The patterns indicate comparable crystallinity for the scaled COFs. Laboratory scale: 1 mL reaction volume (12 – 18 mg of product); Scale up: 100 mL reaction volume (1.2 – 1.4 g of product).

To provide another potential pathway of scaling, the team reports the synthetic scaling of COFs by reflux method (Fig. 9). The translation of traditionally solvothermal synthesis conditions to a reflux setup was monitored based on the crystallinity of the synthesized material, which was comparable to previous results based on the PXRD pattern. Importantly, the reaction mixture was kept under inert conditions (N_2) while the solvent was allowed to reflux from an 80%-filled round-bottom flask. The overall yield of a reaction with 800 mL reaction volume was 14.4 g (yield = 79.9%) of COF-506, which is comparable to the yield of previously reported solvothermal syntheses for this COF.

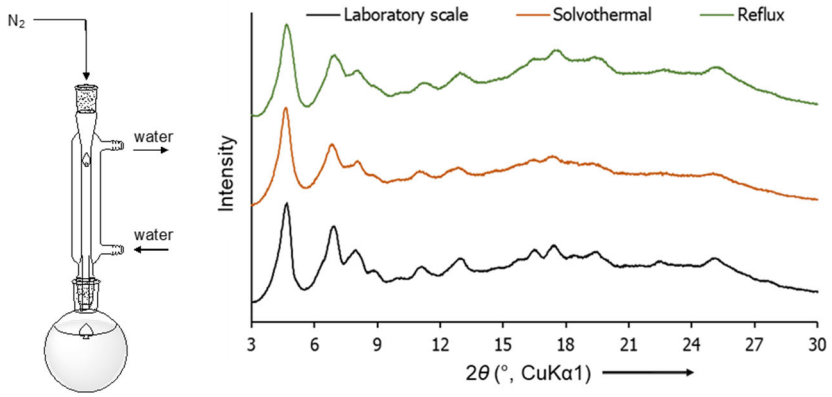

Figure 9. Typical setup for scaling COFs under reflux conditions (left). Comparison of PXRD patterns of woven COF-506 synthesized from solvothermal and reflux conditions (right).

2.1.4 Novel approach to demetalation of COFs & metal recovery

Addressing the goal of metal ion recycling, the UC Berkeley team investigated alternative options to completely remove the copper ions from the COF structures. Whereas the use of potassium cyanide has already been reported to yield demetalated woven and interlocked COFs, a method involving less dangerous chemicals would be preferable.[6-8] Furthermore, the currently employed process requires 3 days to complete, which would be potentially shortened using different demetalation methods.

The team quickly ruled out the use of cyanates (e.g., thiocyanate, isocyanate). Neither of these chemicals could successfully remove the copper ions for the COF structures in temperature ranges from room temperature to 80 °C over the course of 3 days. The use of ethylenediamine has been reported for successful metal ion removal in catenanes.[10] Unfortunately, the use of amines in the presence of imine-linked COFs has also been linked to the exchange of linker between the amine species, thereby interfering with the integrity of the woven and interlocked structures. To prevent linker exchange reactions from occurring during a potential demetalation with ethylenediamine, a post-synthetic modification to a chemically stable functionality (e.g, amide, amine) must be employed. Both the oxidation from imine to amide and the reduction to amine have been reported.[11-13] The oxidation process usually takes at least 3 days to complete, whereas the reduction only takes 1 day to complete. This makes the reduction from imine linkage to amine linkage highly preferable. As shown in figure 10 (example for COF-500), the UC Berkeley team was able to successfully reduce the linkages to achieve amine-linked woven and interlocked COFs. The change in chemical shift from 156 ppm to 48 ppm in the solid-state NMR spectroscopy clearly indicates the formation of amine species from the imines. This evidence is supported by FTIR spectroscopy, which shows the disappearance of the characteristic imine bond stretch at 1622 cm^{-1} and the emergence of an amine stretch at 1528 cm^{-1}.

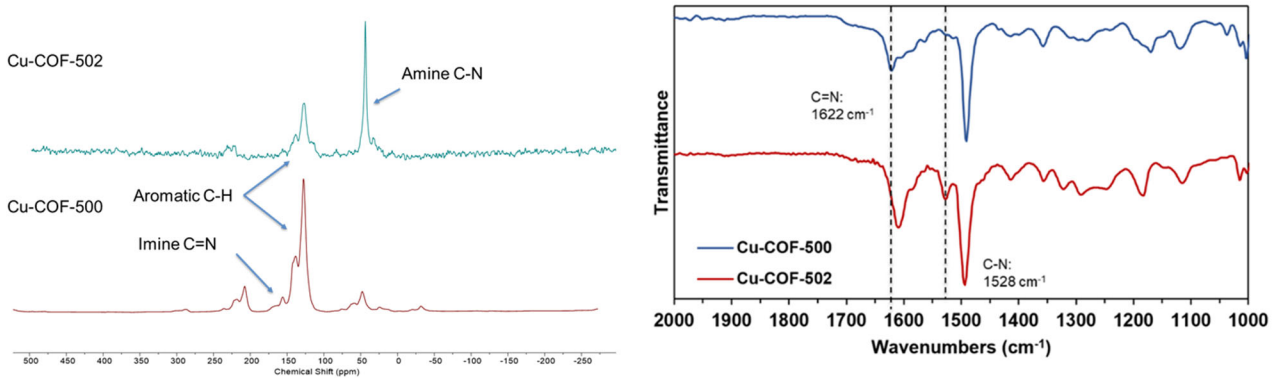

Figure 10. Post-synthetic reduction of imine linkages to amine linkages in Cu-COF-500. Solid state NMR spectra (left) of imine-linked Cu-COF-500 and amine-linked Cu-COF-502 show the disappearance of a characteristic imine-^{13}C signal at 156 ppm and the emergence of a characteristic amine-^{13}C signal at 48 ppm. FTIR spectra of the two compounds (right) confirm these results.

These findings allowed the team to employ a two-step method to chemically stabilize the COF's linkage followed by a copper ion removal using ethylenediamine (Fig. 11). Trials using ethylenediamine to scavenge the copper ions from the structures have proven successful after just 24 h at 70 °C using methanol as a solvent. Importantly, this alternative demetalation process offers not only access to new amine-linked woven and interlocked COFs but also requires less time (-24 h) to complete. The completion of the demetalation process was monitored by inductively coupled plasma atomic emission spectroscopy (ICP-AES), which confirmed the removal of 92-98 % of copper ions. Furthermore, the demetalated amine-linked COFs show a typical change in color from brown to yellow as well as exhibiting substantial loss of crystallinity once the copper ions are removed (Fig. 12).

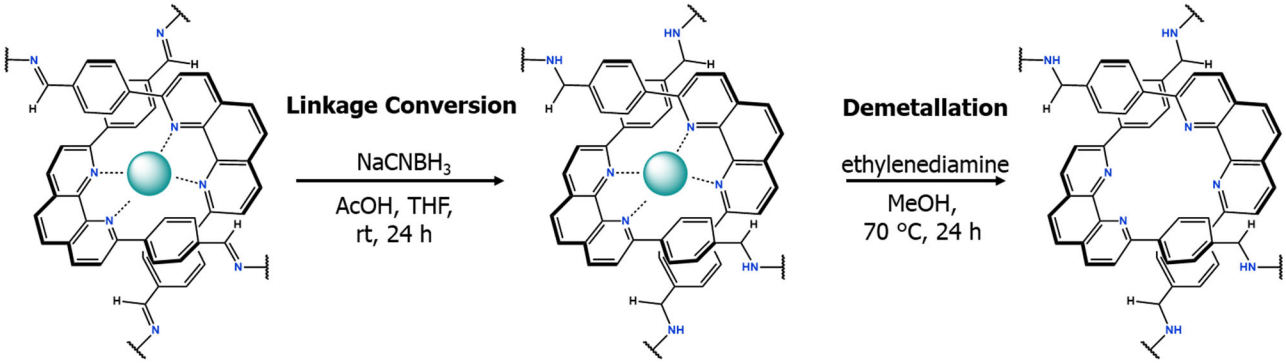

Figure 11. Schematic of two-step process to successfully remove copper ions from the woven structures using ethylenediamine.

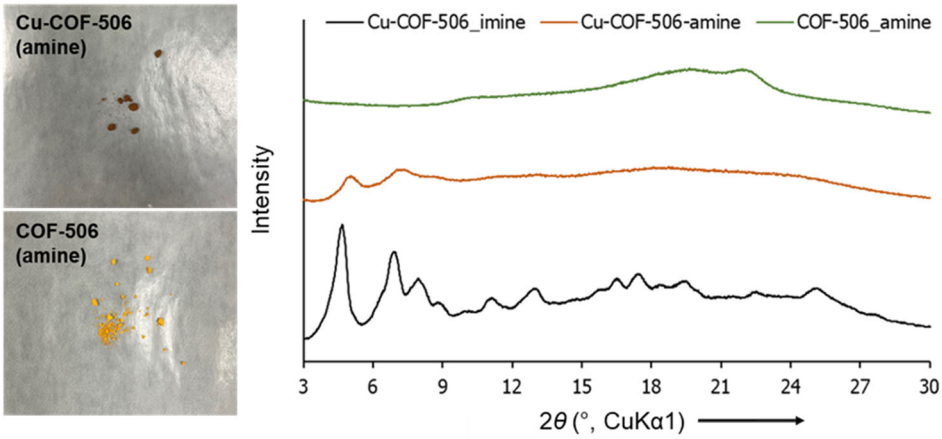

Figure 12. Visible color change of the material before and after the demetalation process (left). Expected loss of crystallinity after post-synthetic modification from imine to amide linkage. Complete loss of crystallinity after demetalation with ethylenediamine (right).

The recycling of the recovered metal ions was performed by chemical reduction of potential Cu(I) and Cu(II) species directly from the demetallation solution.[14] After filtering the aqueous demetallation solution to remove any insoluble impurities, copper ions were reduced by adding an excess of sodium dithionite while stirring under ambient conditions. Within 30 minutes after adding the reducing agent, a discoloration of the reaction mixture was observed, which

coincides with the precipitation of a red-brown solid. The powder x-ray diffraction (PXRD) pattern of the collected recycling product indicates the formation of elemental copper and minimal impurities of copper oxide with a yield of 80 % (Figure 13). Both elemental copper and copper oxide can be used to produce the copper salts used in the synthesis of woven and interlocked COFs.

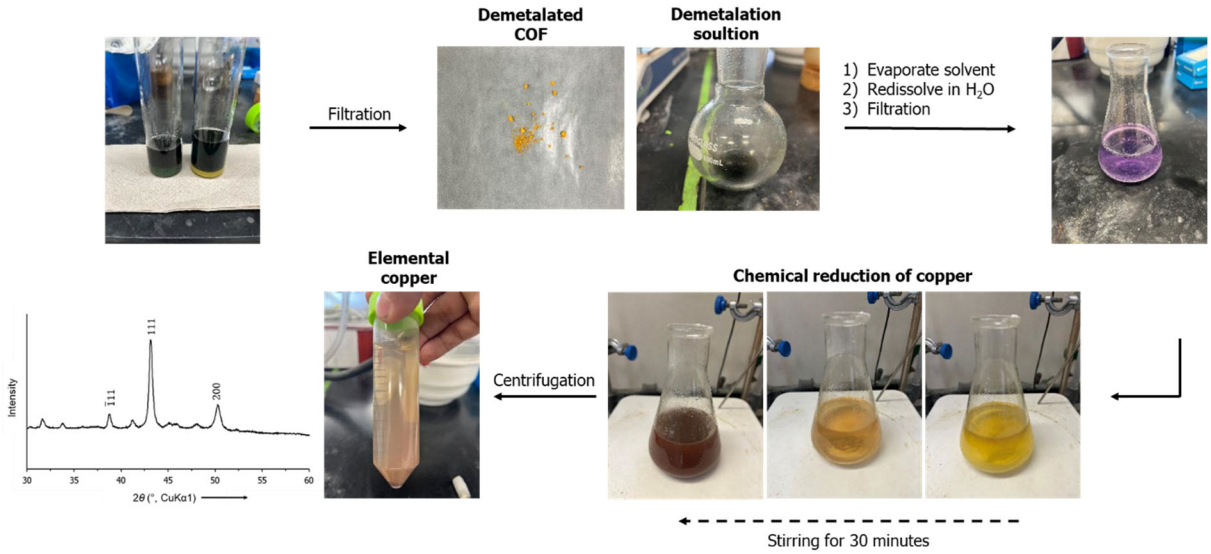

Figure 13. Copper recovery from demetalation solutions. Chemical reduction with sodium dithionite yields elemental copper with traces of copper oxide as shown by the PXRD pattern.

2.2 Synthesis & Characterization of 1D Poly(n)catenane COFs

Beyond the scaling efforts for existing woven and interlocked COF structures, the Berkeley team continued to investigate the potential for MIM polymers originating entirely from COF synthesis. This effort led to the discovery of a new structure that may feature the longest 1D poly(n)catenane chains to ever be reported (Fig. 14).

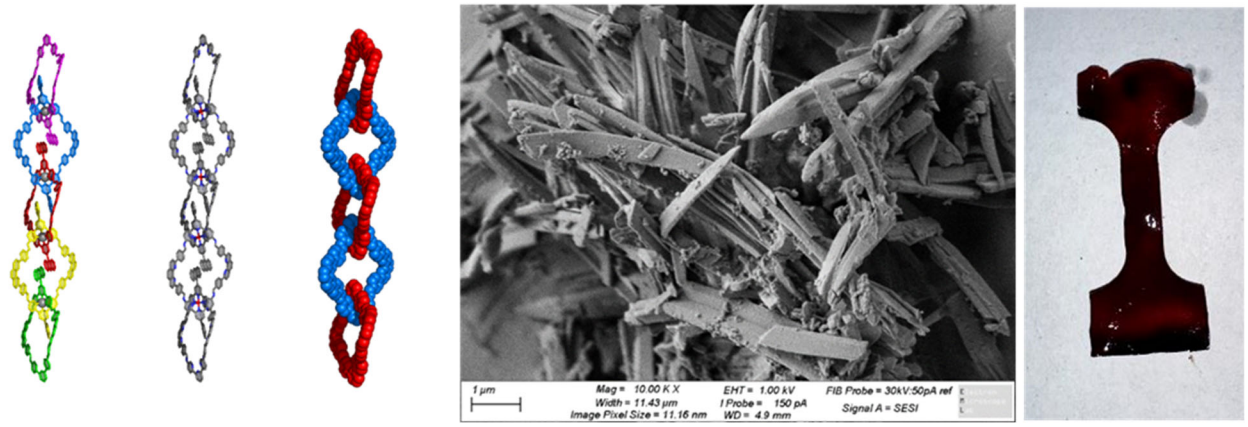

Figure 14. Poly(n)catenane COF. The proposed structure for the interlocked COF suggests the stacking of long 1D polycatenane chains. SEM micrographs of the samples show micron-sized crystals that can be used to generate a polycatenane film.

The COF was characterized by PXRD, FTIR, SEM, and TEM, as shown in figure 15. Importantly, after demetalation and remetalation of the material, the polycatenane structures were able to be molded into dogbones. This level of processability is very important for functional materials and would make it possible to forego the use of polymer composites. However, this material requires further study by techniques such as solid-state NMR spectroscopy, gel permeation chromatography (GPC), and mechanical testing to provide a better understanding of its nature and performance.

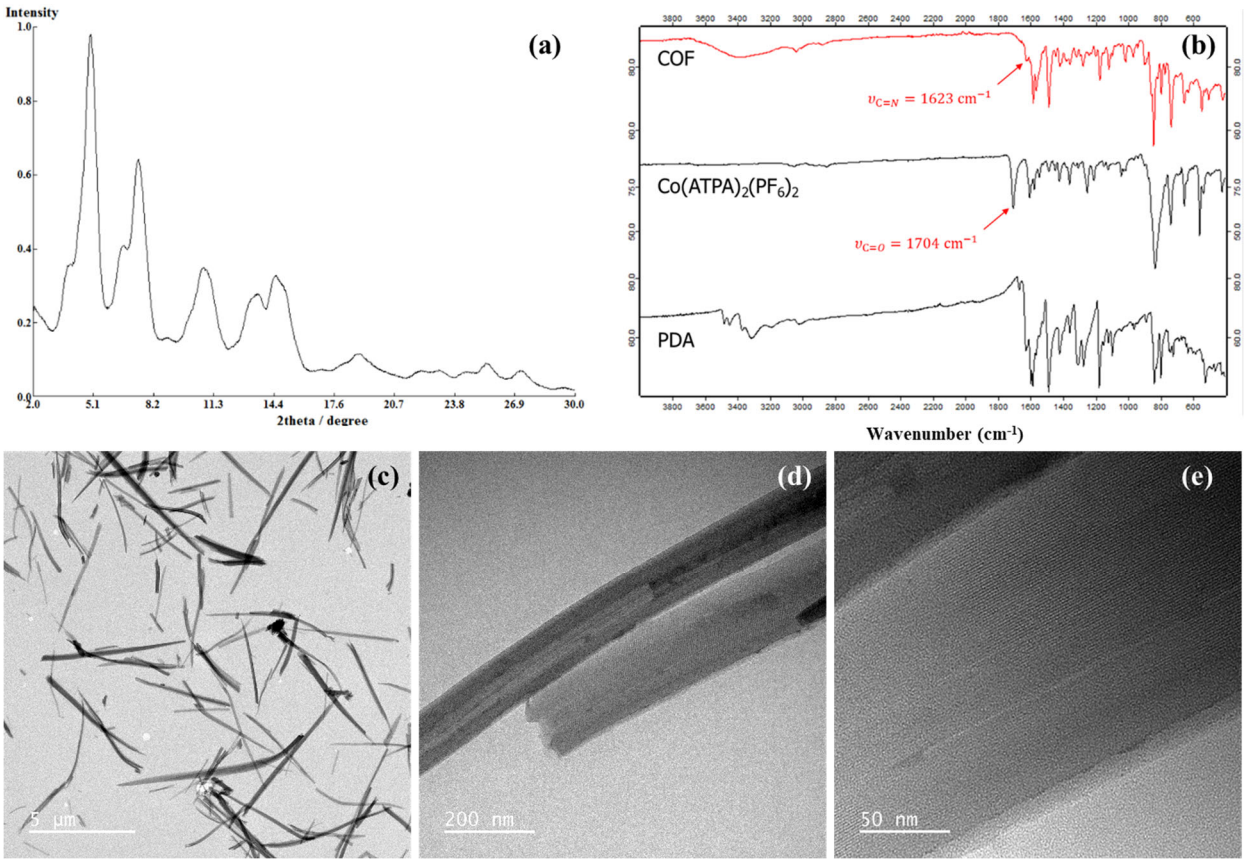

Figure 15. Characterization of Poly(n)catenane COF. (**a**) PXRD pattern of the COF. (**b**) FTIR signals of the COF and its starting materials to provide evidence for the formation of imine bonds. (**c**) Microscopic image of the crystals. (**d, e**) TEM images show lattice fringes that align with the proposed structure.

2.3 Gas & Vapor Adsorption Behavior of Woven & Interlocked COFs

Molecular weaving was examined using a combination of adsorption equilibrium and diffusion rate measurements, and the samples examined for these measurements are slightly different from those used for tensile testing. While in the tensile testing experiments, a small amount of COF was added to the polymer, in the samples prepared for adsorption analysis a ratio of closer to 1:1 polymer to COF was synthesized. (A detailed discussion of the composite synthesis can be found in Section 3.2.) This higher ratio of COF to polymer was examined because it is possible that a polymer containing a small amount of COF may not show weaving behaviors on the per gram basis common in adsorption analysis due to the presence of a large amount of bulk polymer. Therefore, polyimide samples with a COF to PI ratio closer to 1:1 were prepared. The approach then was to utilize the 1:1 sample to observe weaving impacts on the diffusion rates and mechanisms compared to pure, unwoven, COF-506 and physical mixtures of COF-506 and PI.

Diffusion measurements were considered first because the model needed to determine a particular adsorption mechanism is sensitive to material design. Tetrahydrofuran (THF) was used as a probe molecule and concentration swing frequency response (CSFR) was used to measure the diffusion rate on COF-506.

CSFR is a flow-through technique where the adsorbent is equilibrated to a known equilibrium loading and is then subjected to a small, periodic perturbation in the inlet concentration. During this perturbation, the effluent concentration is recorded. The ratio of the amplitudes of the outlet to the inlet, called the amplitude ratio (AR) is plotted against the perturbation frequency (Hz) in a Bode plot. The shape of the response depends on the controlling mass transfer mechanism, and thus with appropriate uptake models, the diffusion mechanism and rate can be determined.

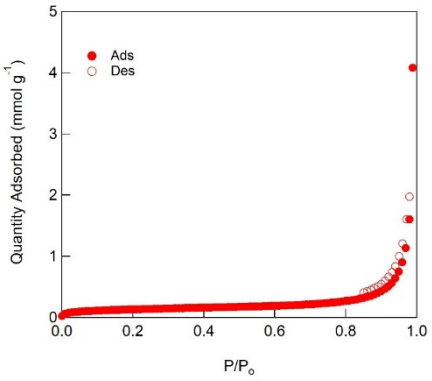

Figure 16. Nitrogen adsorption on COF-506 at 77 K.

The results of this experiment are shown in figure 16 where a micropore diffusion model was used to accurately fit the data. In this experiment, the model lines pass through nearly every experimental data point. The model is then used to extract the diffusion rate, which in this case is $D/r^2 = 1.40x10^{-2}$ s^{-1}. There is very little known about the diffusion of molecules into the structure of COF materials. For comparison, the rate for THF diffusion through the COF is about the same speed as the diffusion of hexane into activated carbon ($2.00x10^{-2}$ s^{-1} at 1.33 kPa) and faster than water diffusion into carbon ($1x10^{-4}$ s^{-1} on average). Diffusion measurements on the woven COF-506/PI, pure PI, and a physical mixture of COF-506 and PI are pending.

Since CSFR data is slower to collect than adsorption isotherms using commercial porosimeters, it was concluded that it may be possible to make a similar conclusion about the impact of weaving by measuring THF adsorption isotherms and comparing the shapes of the adsorption isotherms to determine if PI was loaded into the pore network. Therefore, a nitrogen adsorption isotherm on COF-506 was measured at 77 K using a Micromeritics 3Flex and the BET surface area was calculated to be 10 m^2/g (Figure 17). A low surface area was expected because COF-506 was demetalated, which results in a more closed structure and a loss of crystallinity. However, it is important to recall that COF-506 maintains the ability to expand in the presence of guest molecules and retains adsorption capacity. Further characterization of COF-506, both metalated and demetalated, was performed using light gases such as methane (Figure 18). The very fast diffusion of the light gases through

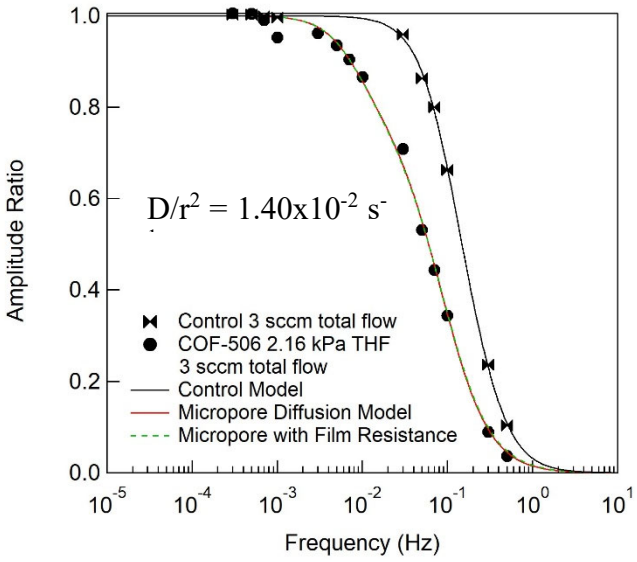

Figure 17. Frequency response of COF-506 at 2.16kPa of THF and 25 °C.

the COF samples made it difficult to quantify by CSFR. Further insight through the collection of isotherms will be necessary to fully characterize the gas adsorption and diffusion behavior of the woven COF.

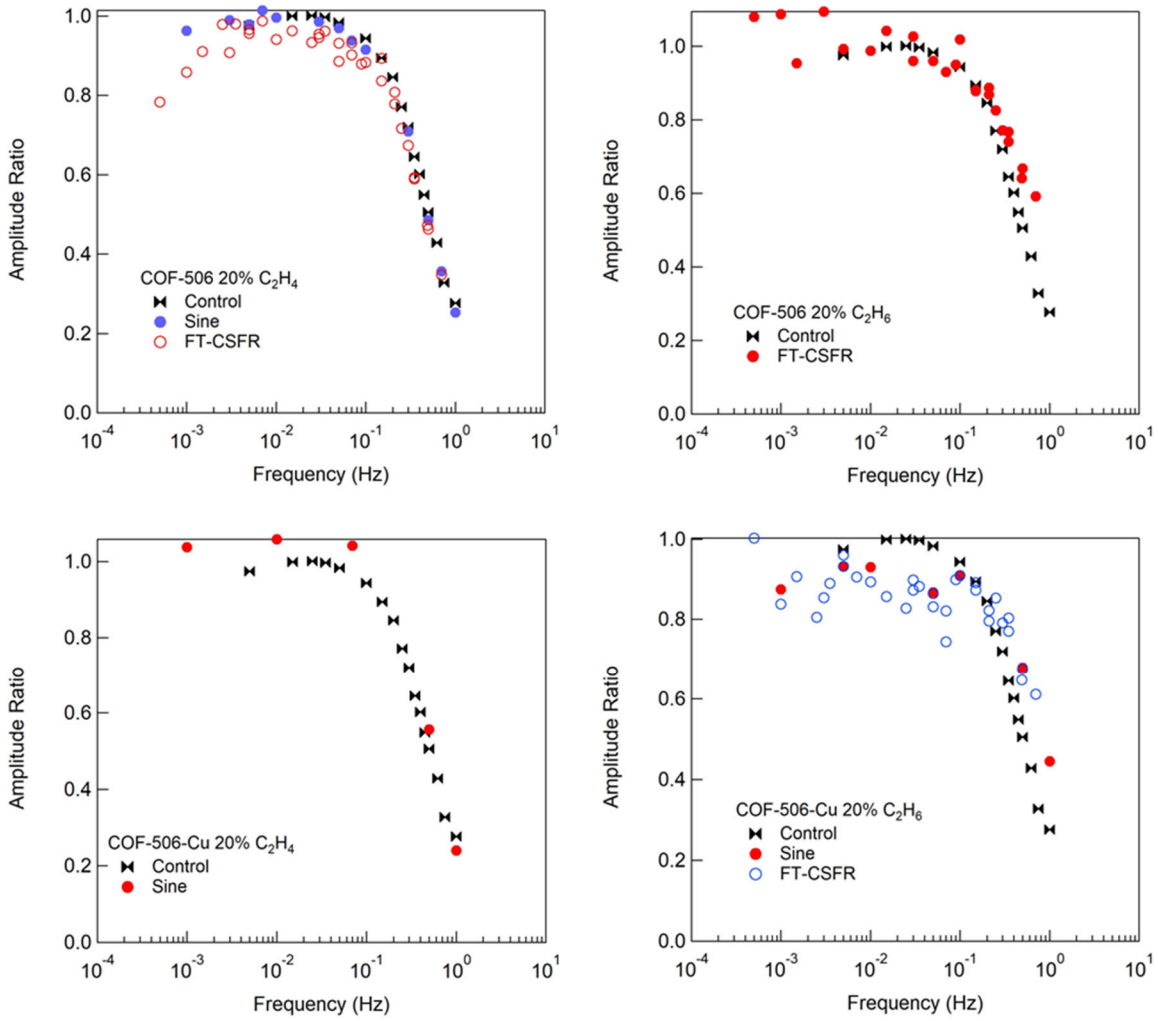

Figure 18. Characterization of COF-506 using light gases. Very fast diffusion of light gases through the COF samples is observed.

3. Polymer-COF Composites

Materials				
Polyimide, Polystyrene, Polymethylmethacrylate with COF 506 and COF 500 initial studies show improved strain behavior as blends and with in-situ polymerization.	Polyimide, Polystyrene, Polymethylmethacrylate, Polycarbonate, Epoxy, Chitosan, and ABS with COF 506 and COF 500	Polyimide, Polystyrene, Polymethylmethacrylate, Polydemethylsiloxane, Polycarbonate and ABS with COF 506 – imine	Polyimide synthesis optimization studies guide optimized temperature, atmosphere, and cure parameters.	Polycarbonate:COF 506-imine composite shows 40% increase in tensile strength with 66% reduction in strain.
	Condensation polymerization and radical cure mechanisms studied. Radicle based mechanisms DO NOT yield polymer in presence of COF imine or amine.	Condensation polymerization and polymer blend systems studied. Stoichiometry study for PI synthesis optimization.	Condensation polymerization optimized but water of reaction has potential negative effect on COF-imines and is hard to remove at this scale.	Polydimethylsiloxane:COF 506-imine composite shows 100% increase in tensile strength and 25% increase in strain capability.
Characterization				
Tensile strength increase measured in PI:COF 506 composite vs virgin polymer from 100 MPa to ~135 MPa.	PI baseline established at 150 MPa and PI:COF composite shows single result of 190 MPa.	NMR end-group analysis technique developed for polyimide synthesis optimization.	Variation in tensile data reduced below 5%	Particle-matrix interphase SFE and viscosity study shows surface interaction between the polymer and COF in solution.
	ABS and PC show promising improvements in tensile strength with COF 506-imine.	Preliminary viscosity studies for understanding PI polymerization support NMR data and allow faster screening.	Rheology of PI precursor solution correlated to tensile strength	Johnson–Kendall–Roberts (JKR) theory analysis
		Model compound ODA-DPI and 2:1 COF infusion prepared for adsorption studies.		Surface roughness analysis is demonstrated to be well correlated to tensile properties
		FT-IR studies indicate COF may be degrading or is sequestering during film preparation.		Surface free energy methodology developed analysis of PC and PDMS films show correlation with tensile strength.

Figure 19. Summarized progress on polymer-COF composites.

3.1 Background

3.1.1 Effect of nanoparticle loading on the tensile strength.

The effect of nanoparticle loading on the tensile strength of interlocked nanoparticle-polymer composites is complex and can depend on a variety of factors such as nanoparticle size, shape, concentration, and distribution within the polymer matrix.[15, 16] However, in general, increasing the nanoparticle loading can lead to an improvement in the tensile strength of the composite material, up to a certain threshold beyond which the strength may begin to decrease due to aggregation or other factors. The addition of interlocked nanoparticles to a polymer matrix can lead to improvements in the mechanical properties of the composite material, including tensile strength, as the nanoparticles can act as reinforcing agents that help to distribute stress more evenly throughout the material.[17] However, the optimal nanoparticle loading, surface chemistry, and distribution within the polymer matrix need to be optimized to achieve the desired properties.

In related work the mechanism of interfacial bond breaking with polymer infiltration into interlocked metallic nanoparticles was shown to be a complex process that could be influenced by several factors such as the nature of the polymer, the size and shape of the nanoparticles, and the

processing conditions.[18-20] When a polymer solution is added to a dispersion of interlocked metallic nanoparticles, the polymer molecules can infiltrate into the spaces between the nanoparticles and form a polymer layer on the surface of the nanoparticles. This can weaken the interfacial bonding between the nanoparticles and the polymer matrix. The degree of weakening can depend on the polymer-nanoparticle interaction, as well as the size and shape of the nanoparticles. As the polymer diffuses into the nanoparticle network, it can also form physical entanglements with the nanoparticles. These entanglements can function as stress concentrators, leading to the initiation and propagation of cracks at the polymer-nanoparticle interface. The formation of voids and defects can also occur due to the formation of a concentration gradient of the polymer within the composite, resulting in an uneven distribution of stress within the material. Furthermore, when the polymer is cured or solidified, the shrinkage of the polymer can further induce stresses at the interface, leading to further interfacial bond breaking. When not optimized, the infiltration of polymer into interlocked metallic nanoparticles could weaken the interfacial bonding, resulting in a reduction in the mechanical properties of the polymer composite.

3.2 Synthesis of Polymer-COF Composites

3.2.1 Experiment F2701-95: Polyimide synthesis

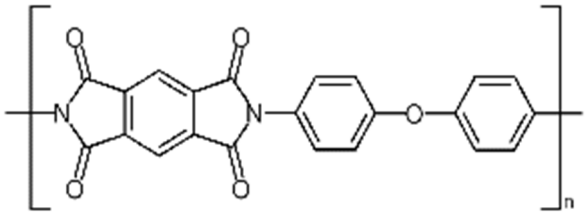

Figure 20. Molecular structure of PMDA-ODA polyimide.

The first attempt to prepare a baseline PI polymer targeted 10 grams of polymer dissolved in N-methylpyrrolidone (NMP) at 13.5% by weight. At this scale there would be sufficient material for repetitive testing and be able to retire early the risks associated with scaling up a polymer synthesis. 5.4779 grams of pyromellitic dianhydride (PMDA) and 5.0137 grams of oxy-diphenyl aniline (ODA) were added to an oven dried round-bottomed flask. 69 grams of anhydrous NMP was added to the flask via canula and stirring was attempted. It was discovered that the PMDA is not soluble in NMP at room temperature and heating was required to dissolve the PMDA. Gentle heat was applied to the flask with a heat gun until all the monomers were in solution. Rapid reaction of the monomers formed a viscous polymer solution. Unfortunately, some imidization of the polymer had also occurred resulting in polymer gels which could not be removed and caused defects in the subsequent films. Several modifications were identified to improve the process based on these results.

1. ODA was first dissolved in dry NMP.
2. PMDA in NMP was slowly heated with stirring until the PMDA was nearly all in solution.
3. ODA solution is added slowly to the PMDA to avoid exotherms.

3.2.2 Experiment F2701-100: Polyimide synthesis

A second high-quality PI polymer solution using fully soluble stock solutions of PMDA and ODA prior to mixing was attempted. The result of this experiment was an extremely low viscosity PI solution. The PMDA solution was stored warm for several hours prior to use and darkened over time. It was reasoned that the PMDA monomer was unstable under these conditions and would need to be used immediately upon dissolution.

3.2.3 Experiment F2701-103: COF-polyimide synthesis

On the third attempt the PMDA stock solution was heated only briefly prior to use. Additionally, approximately 2.5 wt.% of COF was added into the polymer to begin assessment of the COF blending procedure. The COF and monomer component amounts are shown in table 3. COF in NMP was sonicated in a sonic bath for 1 hour and then with a sonic horn for an additional 15 minutes. ODA stock solution was added with stirring and then PMDA stock solution was added. After addition of the monomers, all the COFs appeared to be in solution except COF-500 which still had some large particles. The COF-polyimide solutions are shown in Figure 11.

Table 3. COF and monomer composition, stoichiometric ratio (r), and % COF loading in cured films.

	COF (mg)	ODA sol (g)	ODA (mmol)	PMDA sol (g)	PMDA (mmol)	r	% COF
COF 525	0.0580	8.3323	5.0033	6.6340	5.0149	1.0023	2.768%
COF 505	0.0567	8.3194	4.9956	6.6233	5.0069	1.0023	2.710%
COF 500	0.0516	8.3118	4.9910	6.6240	5.0074	1.0033	2.467%
COF 506	0.0519	8.3082	4.9889	6.6142	5.0000	1.0022	2.484%

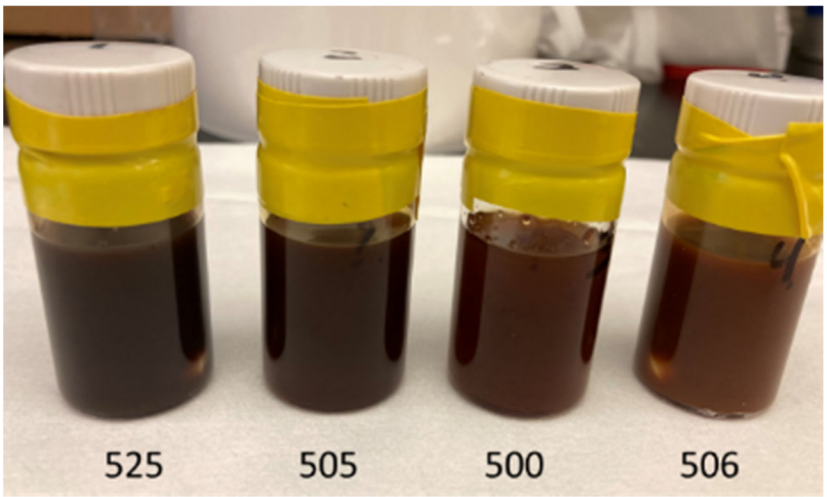

Figure 11. COF-polymer composite solutions.

Addition of PMDA caused rapid polymerization with an increase in viscosity. The COF-polymer solutions were heated at 75 °C for 2 hours then left to cool overnight while stirring. Films were cast from the solutions and the tensile strength measured. Films shown in figure 22, note the observable particles in the COF-500 film.

Figure 22. (left-to-right) GE Research Global Research Center (GRC) polyimide control, polymer composites with COF 500, 505, 506, 525.

3.2.4 Experiment F2701-107: Polyimide synthesis

Incorporating learnings from the prior experiments another 20-gram polyimide synthesis was attempted at a stoichiometric ratio of 1.0015. Films were cast for tensile strength analysis. An additional set of films were prepared using the Sigma Aldrich (PYRE-ML) resin and cast for tensile strength analysis.

Figure 23. GRC synthesized polyimide (PI) film (top). Sigma-Aldrich (PYRE-ML) PI film (bottom).

3.2.5 Experiment F2701-109/110: COF-polyimide synthesis and COF-polyimide blends

COF-500 and COF-506 were ground using a mortar and pestle according to the procedure provided by UC Berkeley to provide a fine powder prior to incorporation into the synthesized COF-polyimide composite at 3 wt.%. Additional samples of COF-500 and COF-506 were milled

in NMP and used to prepare the COF-polyimide blends. Optical images analysis of the cured films is shown in figure 23. In both cases milling was more successful at reducing the COF particle size than grinding by hand. COF-500 proved to be larger than COF-506 under both particle size reduction methods. Films shown in figure 24 show improved COF dispersion and transparency. Both films prepared from COF-500 exhibited dewetting from the glass casting plates.

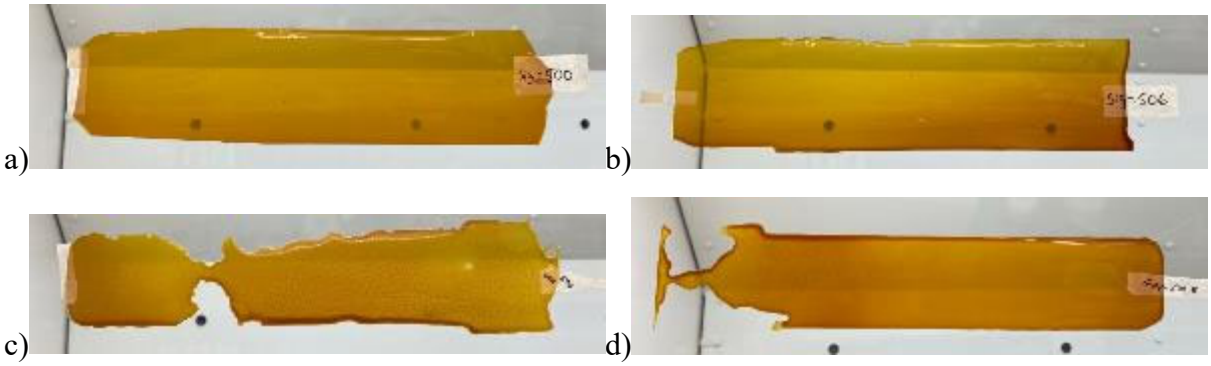

Figure 24. a) Sigma-COF 500 polymer blend, **b)** Sigma-COF 506 polymer blend, **c)** GRC as synthesized COF 500 polymer composite, **d)** GRC as synthesized COF 500 polymer composite**.**

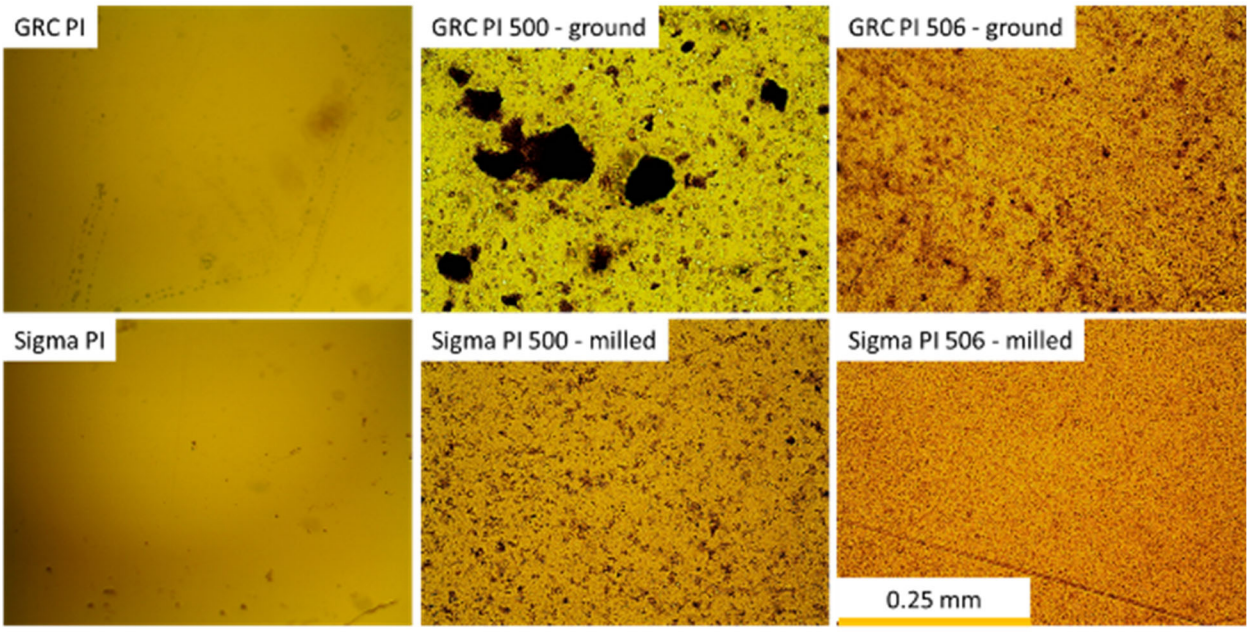

Figure 25. Optical microscopy images of F2701-107/109/110 films.

3.3 Initial Thermomechanical Testing of Polymer-COF Composites

3.3.1 Tensile test benchmarking using commercial Kapton® polyimide

The first task in the thermomechanical testing of the prepared polymer films was to validate the tensile test method using commercial grade Kapton® polyimide film. A 50-micron thick sheet

of Kapton polyimide film was purchased from McMaster-Carr. ASTM D-1708 type test articles were punched from the film and evaluated under tensile load at a strain rate of 1 mm/minute.

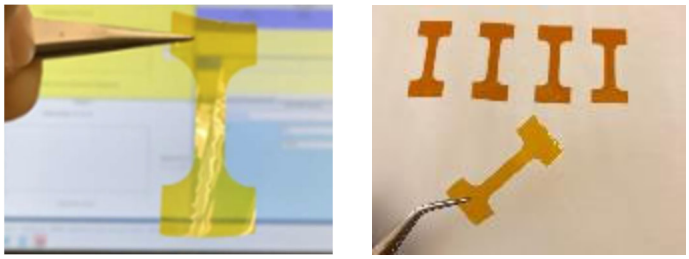

Figure 26. UCB D-1708 microtensile test specimen *(left)*, GE Research D-1708 test specimens *(right)*.

The graphical results of the tensile tests are shown in figure 28. The average tensile stress at break for the five specimens was determined to be 218 MPa +/- 11 MPa. The high quality of the commercial film resulted in a low standard deviation of 5%. The specification for the film was given as 231 MPa, somewhat higher than we measured, however the specification provided by DuPont used the larger D-882 type specimen which was unsuitable for our work due to its large size. Given the good correlation to the accepted value we believe we have a good method in place for film evaluation.

A 13.5 wt.% solution of PYRE-ML resin was used to determine the correct film casting protocol to achieve a 50 to 75-micron thick film. The PYRE-ML solution was cast onto glass plates using a doctor blade at four different thicknesses at a rate of 30 mm/second. The cast films were dried at 75 C overnight followed by curing using a cure profile of 1 hour at 100, 200, and 300 degrees with 100 C/hour ramps. The samples were allowed to cool in the furnace overnight. The cured films were removed from the glass plates by floatation in water then set to dry at room temperature overnight before die cutting and tensile testing. The optimal thickness was determined to be approximately 50 mil (1.27 mm). This was later reduced to 40 mil (1.0 mm) as our film quality improved.

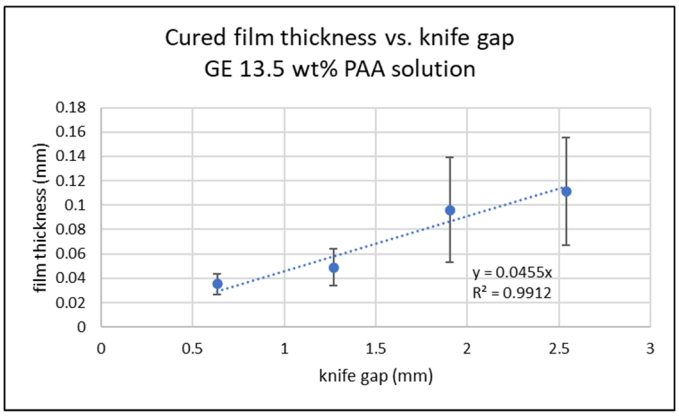

Figure 27. Results of film thickness study using 13.5 wt.% PYRE-ML solution.

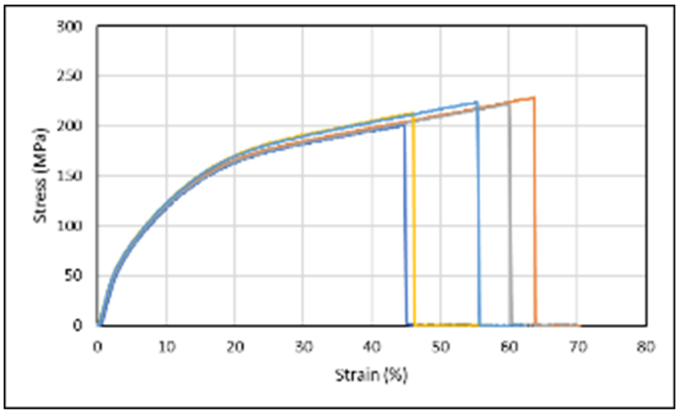

Figure 28. Tensile Test results on Kapton® polyimide films.

3.3.2 Evaluation of GRC polyimide F2701-95

The polyimide film prepared from GE Research Global Research Center (GRC) polyimide F2701-95 had high viscosity indicative of good molecular weight build but also had polymer gels which led to a mottled texture in the cured film and compromised the mechanical strength under tensile test. Filtration of the resin failed to significantly improve the quality of the cast films. Only two of the 5 prepared specimens yielded valid tensile test results and the tensile strength was lower than expected at ~100 MPa (Figure 30). It was determined that the quality of the polymer solution was too low to continue evaluation.

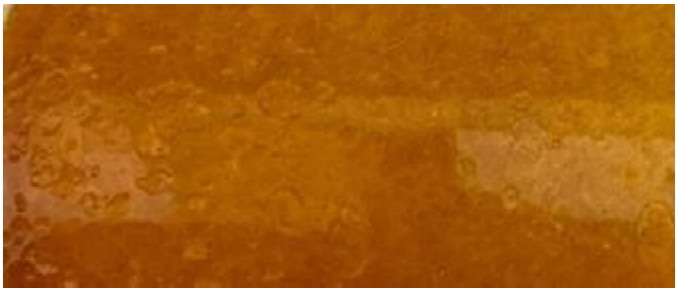

Figure 29. Polyimide film prepared from GRC F2701-95 polyimide.

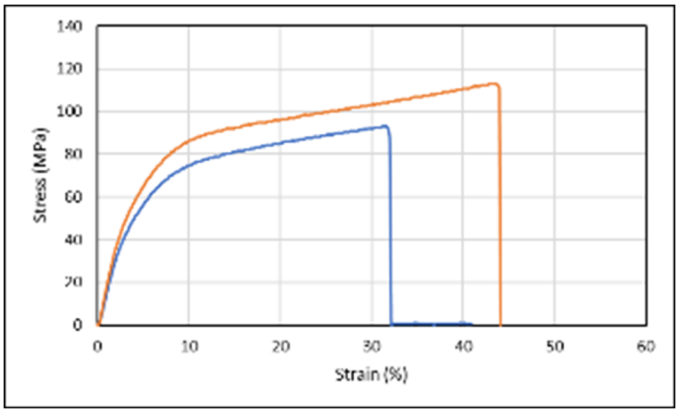

Figure 30. Tensile test results of GRC polyimide F2701-95.

3.3.3 Evaluation of GRC F2701-103 COF-polyimide composites and Sigma-Aldrich PYRE-ML

Six new polyimide films were evaluated from a freshly synthesized polyimide (GRC PI 2), Sigma-Aldrich PYRE-ML (Sigma PI 1) resin, and GRC synthesized COF-polyimides (COFs 500, 505, 506, and 525). Specimens were prepared and evaluated, however the results of all the as-synthesized samples were very scattered. Only the Sigma-Aldrich PYRE-ML film had a tight distribution of data. The approximate tensile strength of that film was determined to be approximately 130 MPa. Due to the large variance values are not reported for the other films, however the tensile traces are presented in figure 31 for reference.

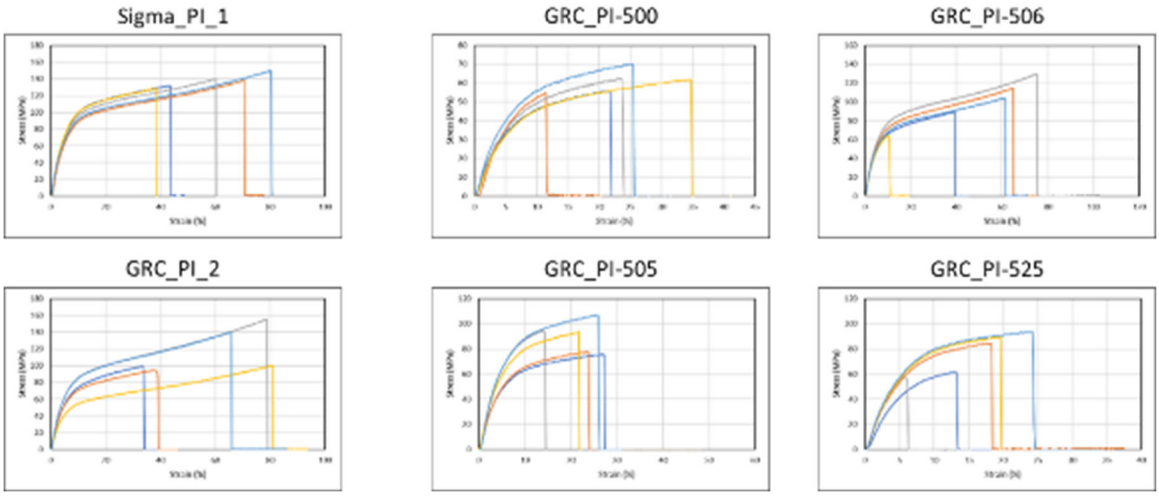

Figure 31. Tensile test traces for GRC F2701-103 COF-polyimide composites and Sigma-Aldrich PYRE-ML.

Optical microscopy of the composites revealed that the COF particles were not well dispersed in the polyimide films (Figure 32). This data supported the assertion from UC-Berkeley indicated that sonication alone was not sufficient to reduce the COF aggregates and physical grinding would be necessary to sufficiently reduce the COF particle size. At the sizes in the micrographs the COF aggregates were likely behaving as defects rather than reinforcing bodies.

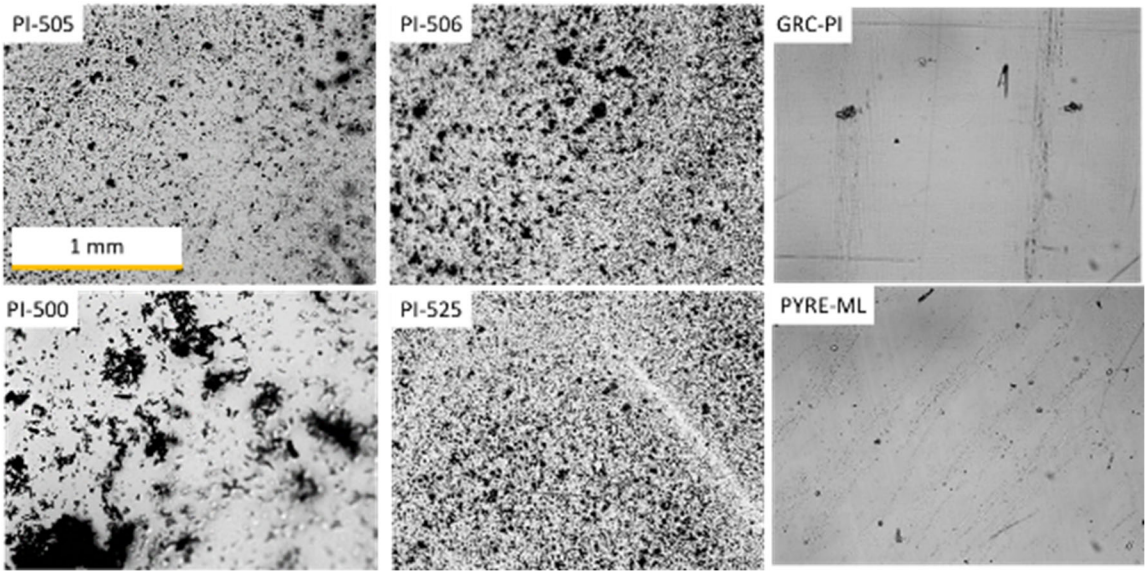

Figure 32. Optical micrographs of GRC F2701-103 COF-polyimide composites and Sigma-Aldrich PYRE-ML.

To assess a better method of reducing the size of the COF aggregates COF solutions in NMP were prepared using shear mixing, sonication, and milling. As shown in figure 33 milling was the best method and provided a solution substantially free from large aggregates. There was concern that milling was too aggressive and may damage the COF structure. Ideally the COF structure would be synthesized at a sub-micron size. In the interim milling was chosen as the best method for COF size reduction.

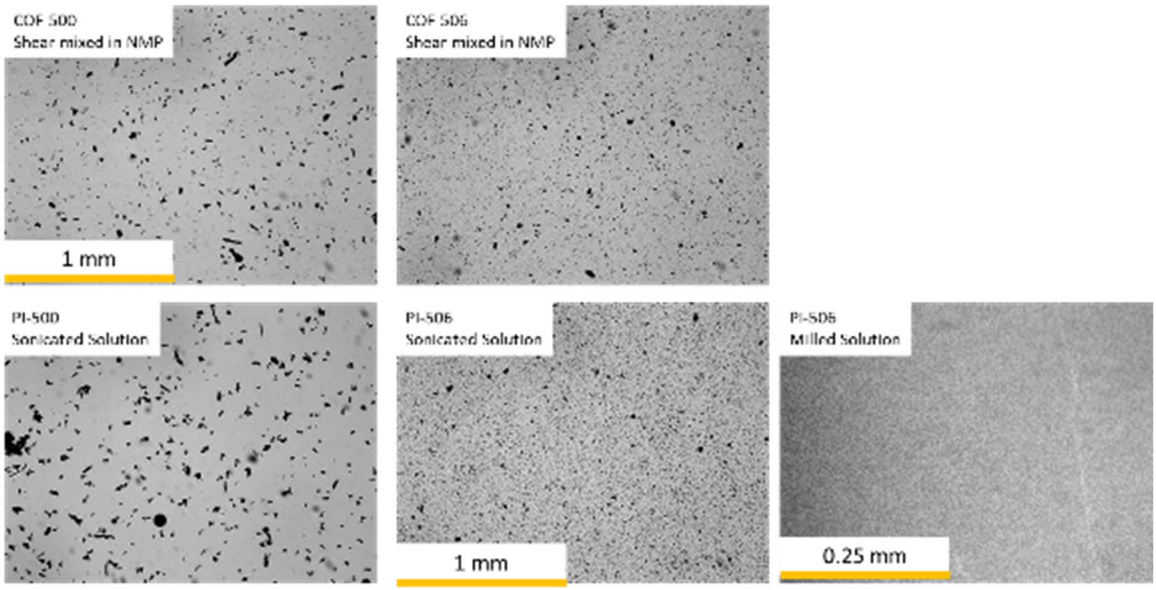

Figure 33. Optical micrographs of COF solutions after shear mixing, sonication, and milling.

3.3.4 Evaluation of GRC F2701-109/110 COF-polyimide synthesis and COF-polyimide blends

Evaluation of freshly prepared GRC synthesized polyimides, Sigma-Aldrich PYRE-ML cast films, COF-500 and 506 PI blends and COF-500 and 506 as synthesized composites was

prepared using ground and milled COFs as described earlier. By thoroughly reducing the particle size of the COFs, defects were avoided. For each of the films 10 to 15 tensile tests were performed. The results of the best five specimens for each film are shown in figures 34 and 35.

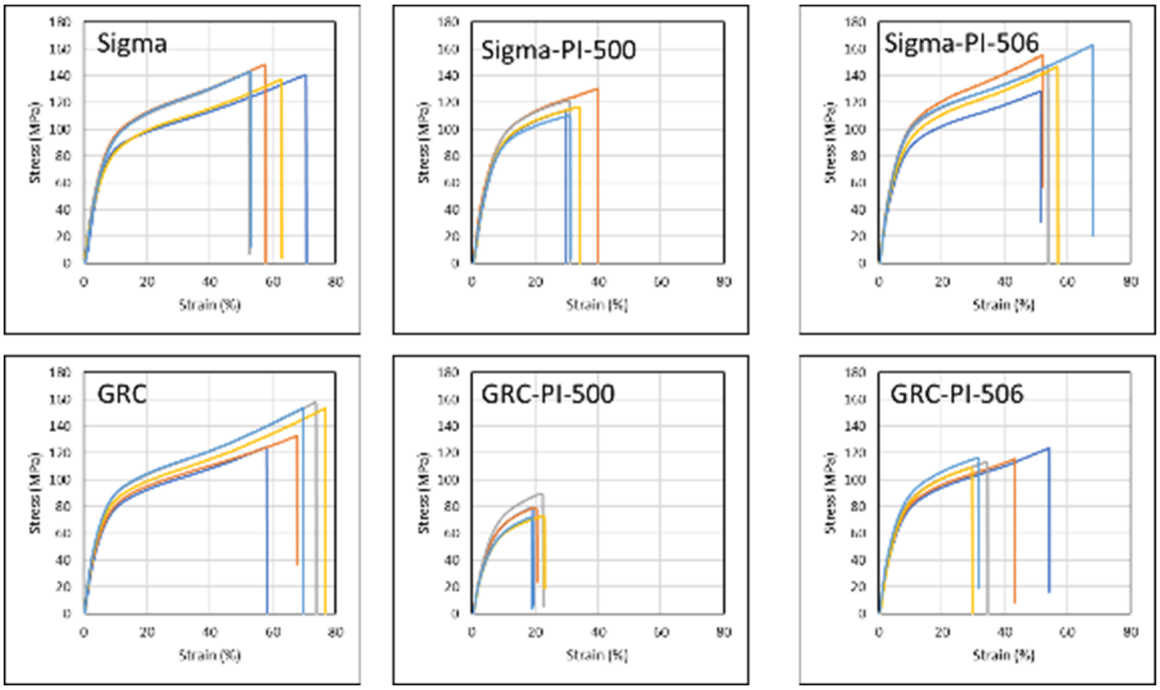

Figure 34. Tensile test results for GRC synthesized polyimide, Sigma-Aldrich PYRE GRC PI 500 and 506 as synthesized composites, and Sigma-Aldrich PYRE-ML COF 500 and 506 blends.

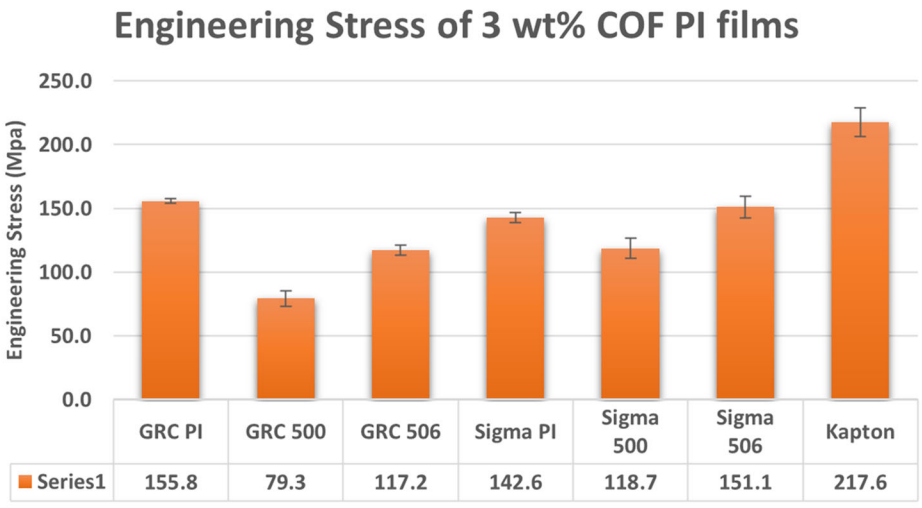

Figure 35. Tensile Stress results for the best 5 specimens for the unfilled and COF-composite films.

The results of the tensile tests demonstrate that the GRC synthesized polyimide is equivalent to the PYRE-ML commercial polyimide. Of the COF samples evaluated, COF-506 outperformed COF-500 with the Sigma-Aldrich (Pyre-ML)-COF-506 blend slightly outperforming the control sample with the same base resin. The control resins and the Sigma-

Aldrich (Pyre-ML)-COF 506 blend outperformed the similar materials in the prior DARPA solicitation.[i] None of the specimens had performance equivalent to the commercial Kapton® film.

3.3.5 Evaluation of F2701-121 and F2701-122: COF-polymer blends with ABS, PMMA and PS.

Evaluation of the films produced in this experiment included a series of tensile tests conducted at 2 mm/min strain rate which was about 1/10th the rate used in our prior tests. As shown in figure 36, all the unfilled polymers a reduction in strain rate corresponded to a drop in the ultimate tensile strength of the films. For PMMA and PS, materials which lacked a plastic deformation region in our testing, the COF composite films also demonstrated a drop in mechanical strength. However, for ABS and PI, materials which exhibited significant plastic deformation there was *significant improvement* in the ultimate tensile strength of the films. Additionally, there was a marked increase in the modulus of all the COF composites when measured at the reduced strain rate. Apart from PS none of the unfilled polymer films had a significant increase in modulus when the strain rate was reduced. The combination of increased modulus and strength at slow strain rates points toward a strong interaction between the COF and the polymer matrix which we would expect if the polymer were woven into the COF structure.

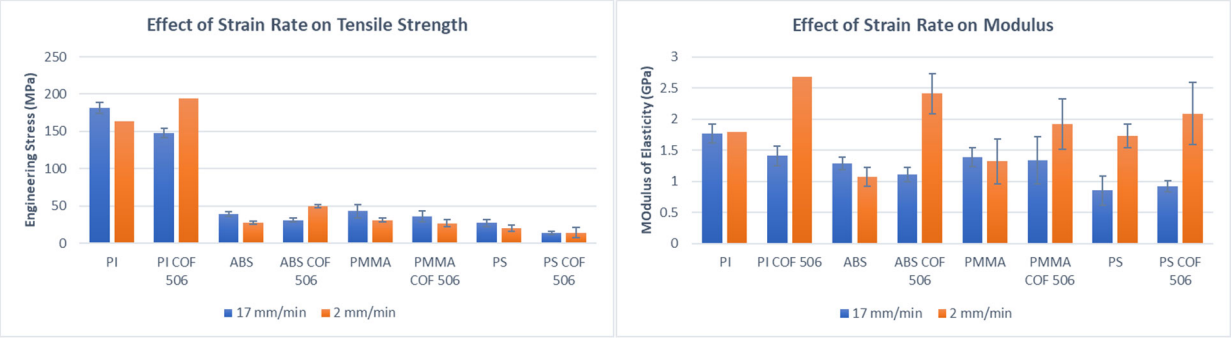

Figure 36. Effect of Strain Rate on the Tensile properties of polymer-COF composite films.

Figure 37 shows the effect on the ultimate tensile strength for the four polymer systems with both COF-500 and COF 506. Consistent with our findings to date COF-500 did not improve and generally degrades the performance of the matrix polymer. This may be due to the difficulty associated reducing the size of COF-500 by grinding or milling and additionally, in the case of polyimide, the loss of molecular weight build.

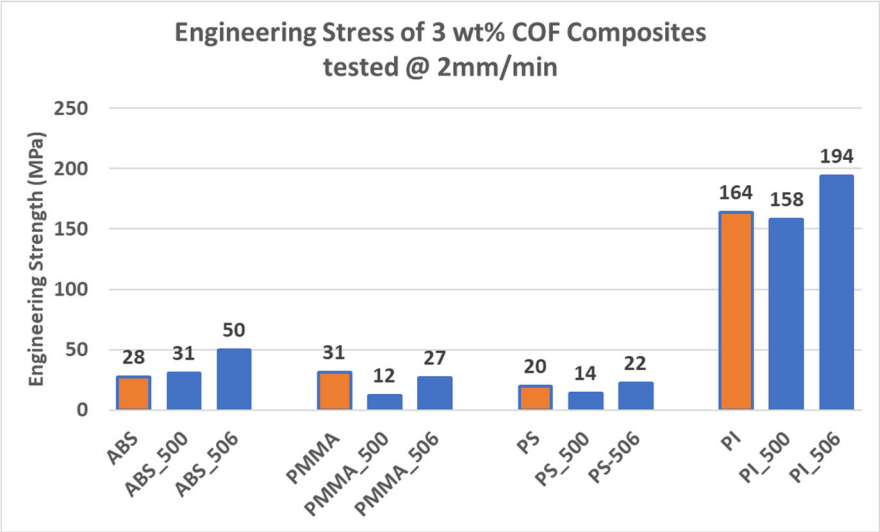

Figure 37. Comparison of ultimate tensile strength of polymer-COF composites evaluated at a strain rate of 2mm/min.

3.3.6 Experiments F2714-5 and F2714-6: Preparation of COF: polymer blends with Polycarbonate (PC).

Blends of polymers with COF 500 and 506 were prepared with chloroform as solvent for film casting and mechanical testing. The COF was first prepared by roll-milling in chloroform with hardened zirconia milling beads for 3 to 5 days until a fine powder was achieved. In the case of COF 500, after 7 days milling hard agglomerates were still present and were removed by passing through a coarse sieve (45 micron). The particle size distribution of these COF materials was analyzed using UV-vis spectroscopy. An optical density profile at 550 nm were performed for both the COF-500 and COF-506 to ensure a monodisperse submicron particle distribution before further processing. At this stage, after milling, polymer solution was added to the milling vial and the vials were further stirred for 24 hours at room temperature then stored overnight (without stirring) to distribute the COF and allow the polymer to diffuse into the COF structure. Films were then cast on glass plates (using and placed in a heated oven at 75 °C to remove the solvent for a minimum of 2 days. The dry films were floated off the glass with deionized water and then dried in air overnight before testing. The Dried films were punched out to standard ASTM sample testing size and used for further tensile testing and analysis. The resulting punched out samples were measured for their average thickness along their gauge length and a pre-programmed analysis tool was used for measuring the tensile strength of these polymer composites using Instron tester. A simple modification was made to the previously reported tensile strength testing method, as follows. The edges of these films, which contact the clamps in the tester, were covered with an insulating 3M tape (to avoid abrasion and impaction due to the clamps inhomogeneous surface roughness).

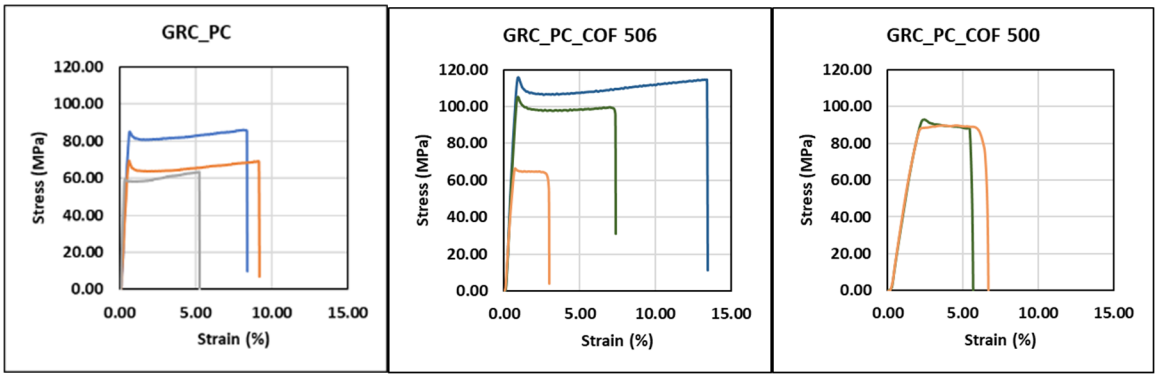

Figure 38. Tensile test results for GRC synthesized polycarbonate composite films with COF-506 and COF-500 impregnation.

The tensile test traces shown in figure 38 show a significant improvement in the yield and tensile strength of the COF containing polycarbonate films like what we had previously seen from the samples prepared from ABS. The COF-506 filler again appears to be a superior structure for enhancing the properties of the matrix polymer. Not surprisingly, polycarbonate also exhibits a significant plastic deformation region which appears to be a critical component for a favorable CO-polymer interaction.

3.4 NMR and adsorption characterization

3.4.1 Experiment F2701-121A: COF-PI at 2:1 ratio.

Elucidation of the weaving of the polymer into the COF structure required the preparation of a COF-PI at a much higher COF loading than in our typical composite studies. For this experiment COF 506 was ground with a mortar and pestle and 101 milligrams was added to a vial containing 104 mg ODA and 2.17 grams of NMP. The vial was stirred for 3 hours at 75 °C and then 113 milligrams of PMDA was added. A viscous suspension of COF rapidly formed. The suspension was stirred overnight then poured into an aluminum pan, dried at 75 °C to remove solvent and then imidized by slowly heating to 300 °C over 6 hours before cooling to room temperature. Retention of the COF structure was confirmed by PXRD. The film was easily removed from the pan and sent to the University of Southern Alabama for analysis.

3.4.2 Experiment F2701-123: Preparation of ODA-DPI

ODA-DPI (oxydianiline-di-phthalimide) was prepared by dissolving 3.3 grams of oxydianiline (16.5 mmol) in 65 mL of anhydrous NMP. 10 grams of phthalic anhydride (67.4 mmol) were dissolved in 50 mL of NMP and added dropwise to the ODA solution. Once the addition was complete the reaction was heated to 75 °C for 24 hours. After cooling the solution was filtered and poured into 400 mL of water where a precipitate formed. The precipitate was collected by vacuum filtration and washed 5 times with 100 mL of isopropanol. The damp cake was transferred to an Erlenmeyer flask and dissolved in hot xylenes:NMP (90:10). The hot solution was filtered to remove residual solids and let cool to room temperature. A yellow-orange solid formed. The

supernatant was poured off and the residual solid was recrystallized from xylenes:NMP to yield 4.6 grams of product in 60% yield.

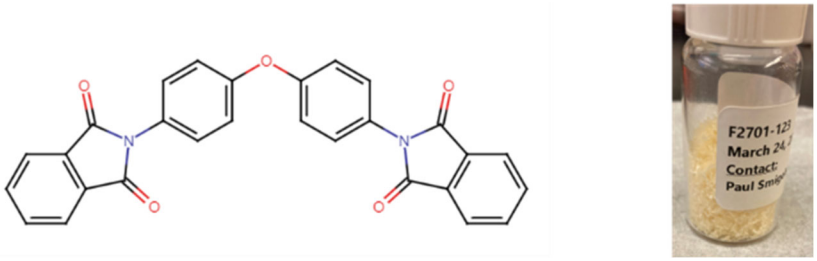

Figure 39. Chemical structure of ODA-DPI and isolated crystals.

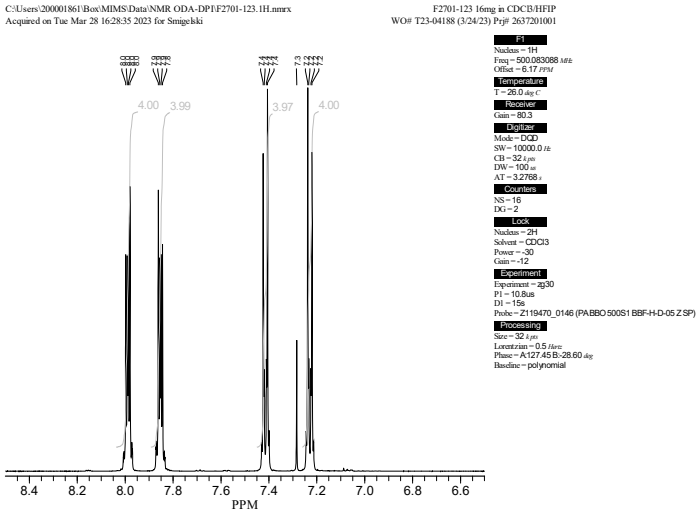

Figure 40. 1H-NMR of ODA-DPI. peak at 7.3 ppm is CDCl3 NMR solvent.

3.4.3 Experiment F2701-124: Small molecule infusion of COF 506

In this experiment COF 506 we attempted to infuse COF 506 with small molecules to demonstrate a change in the adsorption characteristics of the COF when matrix is present in the pore structure. COF 506 was ground with a mortar and pestle to a fine powder. Approximately 85 mg of COF 506 was placed in each of three vials and 90 mg of either styrene, methyl methacrylate, or ODA-DPI, was added to the vial. To the vial containing ODA-DPI we added 200 uL of NMP to dissolve the compound and encourage infusion. To the vials containing styrene and methyl methacrylate we added 200 uL of toluene containing approximately 10 mg of radical initiator. The three vials were sealed and placed in a 75 °C oven overnight then transferred to a 100 °C oven to complete polymerization. Finally, the vials were transferred to a 120 °C vacuum oven to remove residual solvents.

The darkened COF powder was removed from each vial and weighed. The COF-ODA-DPI samples appeared homogeneous, and the weight (189 mg) agreed with theory (191 mg). This sample was ground and sent to the University of Southern Alabama for analysis. The weights of the styrene and methyl methacrylate sample indicated that the monomers had completely evaporated, only residual COF remained. We repeated this protocol a second time including a set

of samples with no COF as control samples. In this iteration the COF free monomers polymerized to dense solids while the monomers again evaporated from the vials with COF. Based on a cursory literature search we believe the imine COF quenches radical polymerization and we will need the oxidized COF to continue with this path.

3.5 Scaled-up Synthesis of Polymer-COF Composites

3.5.1 Experiment F2701-118: Stoichiometry and branching optimization of COF-polyimide composites.

In this experiment an off-stoichiometry and a branched COF-polyimide composite were included to elucidate the effects of branching and to optimize the stoichiometry of the matrix prior to scale-up. Shown in 4 are the formulations used in this study. The stoichiometric ratio (r) should determine the maximal molecular weight this matrix can achieve, with values closer to 1 leading to higher molecular weights.

Table 4. COF-PI formulations for branching and stoichiometric ratio (r) evaluation.

	ODA	PMDA	melamine	r	viscosity	Tensile Strength	St.Dev.
GRC PI Control	1.0007	1.0919	0	0.9983	4380	155.5	11.9
GRC PI LMW Control	1.0001	1.0971	0	0.9930	9280	181.5	6.8
GRC PI Branched	1.0001	1.0981	0.0036	1.0006	7800	160.2	9.0
GRC PI 500	1.0002	1.0973	0	0.9929	250	122.1	7.0
GRC PI 506	1.0002	1.0971	0	0.9931	2358	147.4	6.5

For this series of experiments the weight loading of polymer in solution was held constant therefore viscosity is a reasonable proxy for molecular weight according to the Mark-Houwink Equation (Equation 1), where η is the intrinsic viscosity, K and α are polymer-solvent interaction parameters, and M is the molecular weight of the polymer.

$$[\eta] = KM^{\alpha}$$

Equation 1. Mark-Houwink equation relating inherent viscosity to molecular weight.

Despite the near identical r-values of the LMW, 500, and 506 samples we found significant variation in the viscosity of the polymer solutions, a good indication that the molecular weights were different. Films were cast from the solutions and the mechanical strength was measured by tensile test. Optical images of the dried and cured films are shown in figure 41. Note the slight haze in the film containing COF-500 relative to the clarity of the film made with COF-506.

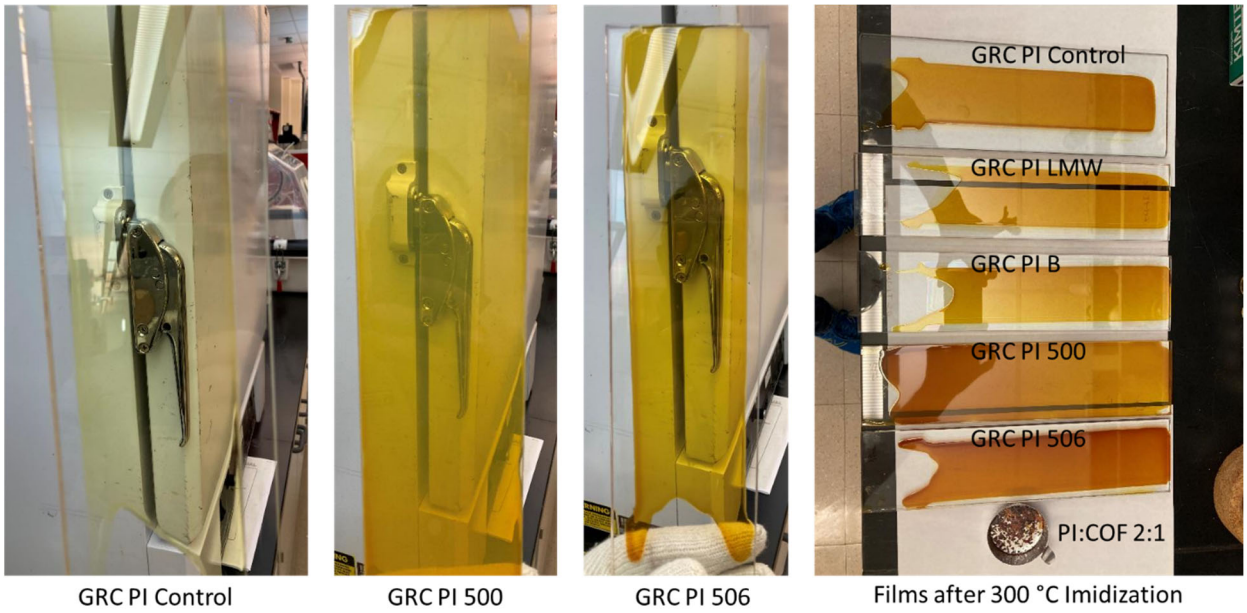

Figure 41. Optical image of PI and COF-PI composite films from Experiment F2701-118.

3.5.2 Experiments F2701-121 and F2701-122: Preparation of COF-polymer blends with ABS, PMMA and PS.

Blends of polymers with COF-500 and 506 were prepared in different solvent systems for film casting and mechanical testing. The COF was first prepared by roll-milling in xylenes with hardened zirconia milling beads for 3 to 5 days until a fine powder was achieved. In the case of COF-500, after 5 days milling hard agglomerates were still present and were removed by passing through a coarse sieve. After milling, polymer solution was added to the milling vial and the vials were further stirred for 4 hours at 75 °C (room temperature for THF samples) then allowed to cool by rolling overnight to distribute the COF and allow the polymer time to diffuse into the COF structure. Films were then cast on glass plates and placed in a heated oven at 75 °C to remove the solvent for a minimum of 2 days. The dry films were floated off the glass with deionized water and then dried in air overnight before testing. Images of the COF-506-polymer blends are shown in figure 42. COF-506 had a unique interaction with ABS in THF resulting in agglomeration of the COF particles. When we switched the solvent to NMP there was no obvious agglomeration although the COF appeared to migrate away from the edges of the film.

Table 5. Composition of COF-polymer blends.

Sample	polymer	solvent	COF	polymer mass (g)	COF mass (mg)	%wt COF
F2701-121a	PMMA	THF	506	3.64	56.8	1.56%
F2701-121b	ABS	THF	506	3.17	53.8	1.70%
F2701-121c	PS	THF	506	3.21	64.3	2.00%
F2701-122a	PMMA	NMP	506	1.01	26.2	2.59%
F2701-122b	PS	NMP	506	0.99	30.8	3.10%
F2701-122c	ABS	NMP	506	1.03	28.3	2.75%
F2701-122d	PMMA	NMP	500	1.01	27.8	2.74%
F2701-122e	PS	NMP	500	1.08	28.2	2.62%
F2701-122f	ABS	NMP	500	1.02	30.1	2.95%

Figure 42. Optical images of COF 506 polymer blends prepared from THF and NMP.

3.6 Polycarbonate (PC) and Poly(dimethylsiloxane) (PDMS)

3.6.1 Preparation of PC and PC-COF films

Blends of polymers with COF 506 were prepared using dichloroethane (DCE) as the solvent for film casting and mechanical testing. COF-506 was initially prepared by roll-milling in DCE with hardened zirconia milling beads for a duration of 3 to 5 days until achieving a fine powder. The particle size distribution of the COF-506 material was assessed using UV-vis spectroscopy. An optical density profile at 550 nm was recorded to ensure the presence of a monodisperse submicron particle distribution before proceeding with further processing. Following the milling phase, a polymer solution was introduced into the milling vial, and the vial was further stirred for 24 hours at room temperature before being stored overnight (without stirring) to facilitate the distribution of COF and allow the polymer to permeate the COF structure. Films were cast onto glass plates and placed in a heated oven at 75 °C to eliminate the solvent over a minimum of 2 days. The dry films were floated off the glass using deionized water and then air-dried overnight before undergoing testing.

Polycarbonate (PC) is known for its favorable qualities when it comes to creating spin-coated films on glass slides, making it the primary polymer of interest in this study. The films of Polycarbonate were prepared using Chloroform and dichloroethane solvents, whereas PDMS was

prepared with a crosslinker (Dow corning). Figures below illustrate the chemical structures of Polycarbonate, and PDMS. It is a well-established fact that when a polymer is exposed to temperatures higher than its glass-transition temperature (Tg), the hydrogen bonds within it are disrupted (beneficial/non-beneficial depending on the interactions). These bonds then reform in a different manner, both intermolecularly and intramolecularly, as the polymer rapidly cools to ambient temperature. Hence, we opted for a thermal treatment temperature of < 120 °C for both the cases.

A 45-micron bilayer film of polycarbonate (PC) was fabricated using a spin caster in a multistage process. The first stage involved the deposition of a 25-micron monolayer of PC solution onto a clean substrate. The spin caster, operated at 2500 RPM for 30 seconds with 10 loops, facilitated the even spreading of the PC solution. Subsequently, the monolayer was allowed to dry overnight to ensure solvent evaporation. In the second stage, a fresh PC solution was prepared, and it was poured onto the existing monolayer. The spin caster, maintaining the same parameters as in the first stage, was employed to create a 20-micron second layer over the monolayer. The resulting bilayer film was then left to dry thoroughly to enable complete solvent evaporation. This process yielded a 45-micron bilayer film of PC, offering enhanced adhesion and improved specific mechanical properties suitable for a range of applications.

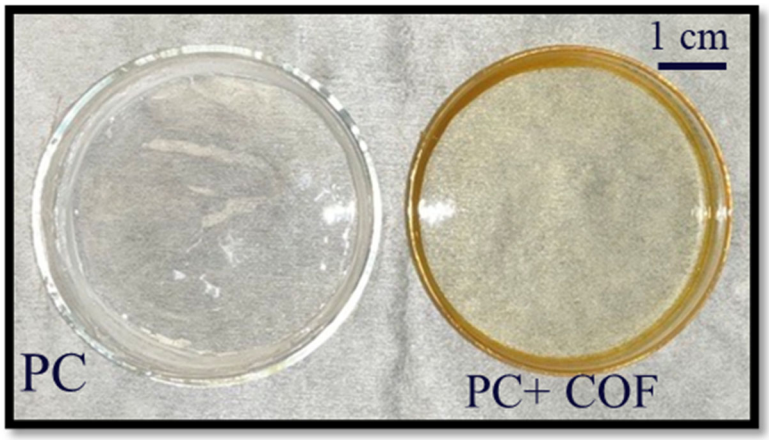

Figure 43. Spin cast films of PC and PC-COF.

The dried films were punched out into standard ASTM sample testing sizes and used for subsequent tensile testing and analysis. These punched-out samples were measured for their average thickness along their gauge length, and a pre-programmed analysis tool was employed to measure the tensile strength of these polymer composites using an Instron tester. A minor modification was made to the previously reported tensile strength testing method, which involved covering the film edges that contact the clamps in the tester with insulating 3M tape to prevent abrasion and impact resulting from the clamps' uneven surface roughness.

a)

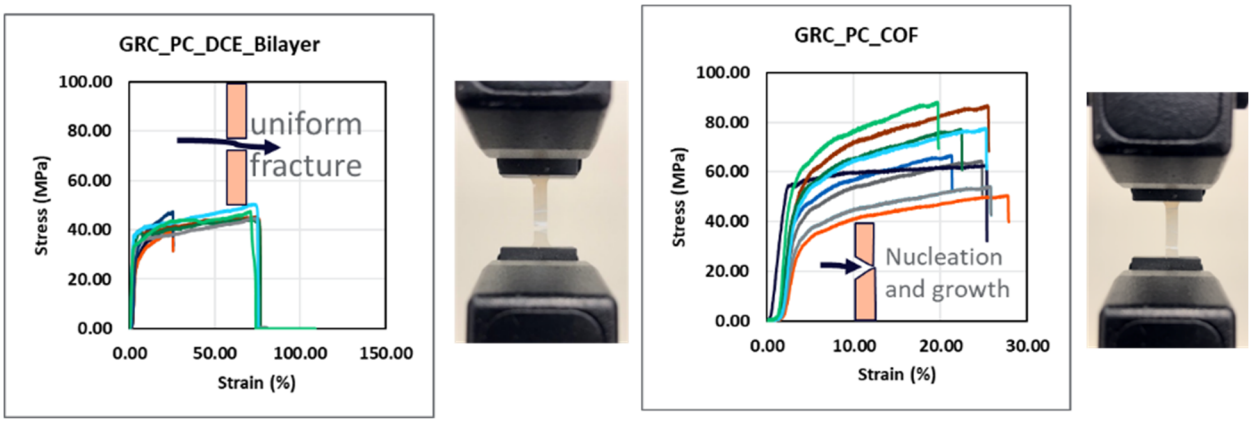

b)

	Young's Modulus	
	Spin Coating	Draw casting
PC_DCE	14.07	15.34
PC_DCE_506	5.70	8.40

Figure 44. Tensile strength testing of PC and PC-COF. a) *left* polycarbonate control samples *right* polycarbonate/COF composite samples. Individual test samples are shown in alternating colors for clarity. **b**) comparison of modulus data for unfilled and composite films prepared by spin and draw casting.

Figure 44a presents the results of the tensile tests in this study. In figure 44a, stress vs. strain graphs for all materials tested are displayed, showing that incorporating the COF in the matrix material enhances its ability to deform before failure, resulting in increased stiffness and higher tensile strength. This observation is supported by Figure b, which provides the calculated tensile strength values. In all cases, the nanocomposites exhibited superior tensile strength compared to the pristine PC polymer. Notably, the most substantial reinforcement was observed in the nanocomposite even with a 3% COF concentration, with a remarkable 41.9% increase compared to the corresponding pure PC polymer value. While the tensile strength decreased in nanocomposites with higher filler loadings, even the highest loading of 6% evaluated in this study exhibited a tensile strength approximately 24% higher than that of the pure PC material. Figure b displays the corresponding young's modulus of elasticity values, which closely mirrored the trends observed in the tensile strength values. The 3% concentration nanocomposite demonstrated a remarkable 50% increase in tensile modulus of elasticity compared to the pure PC material.

3.7 Material Characterization and Synthesis Optimization

3.7.1 Evaluation of GRC F2701-118 COF-polyimide composites

Tensile testing was performed on samples from experiment F2701-118 and the ultimate tensile strength was correlated to the viscosity of the polymer solution measured prior to casting (Figure 45). We found a strong positive correlation between the solution viscosity and the strength of the cast films. PI-COF composites were lower in viscosity and strength than the control samples. Data is tabulated in (Table 4) This is an indication that the strength of the composite and the viscosity of the solution are related to a failure of molecular weight build in the samples with added COF.

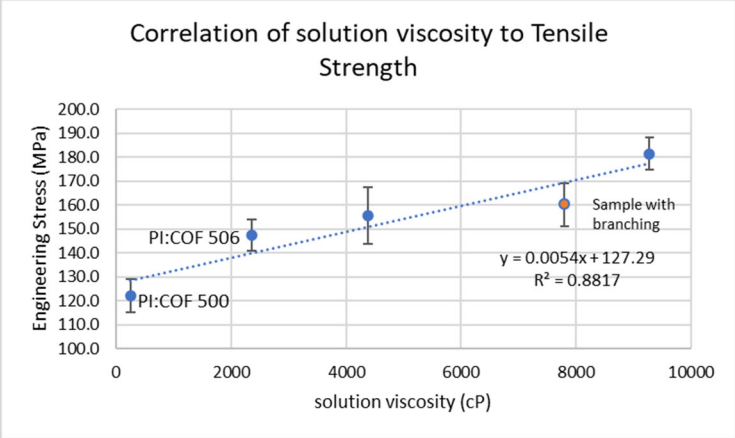

Figure 45. Correlation of viscosity and tensile strength for experiment F2701-118. Data point in orange is the sample with melamine branching agent added.

3.7.2 De-aggregation of COF

COF powder as received proved too coarse for the preparation of thin film samples causing film defects and settling out of solution. Manual grinding, high shear mixing, ultra-sonication, and wet milling were all explored to determine the best way to achieve a submicron powder. Figure 46 shows SEM images of COF-506 crystals which tended to be either random aggregates or nicely formed spherical aggregates. The random aggregates were mainly composed of a distribution of sizes up to about 0.5-micron primary particles where the spherical aggregates tended to be somewhat more monodisperse with an approximate size of 250 to 300 nm.

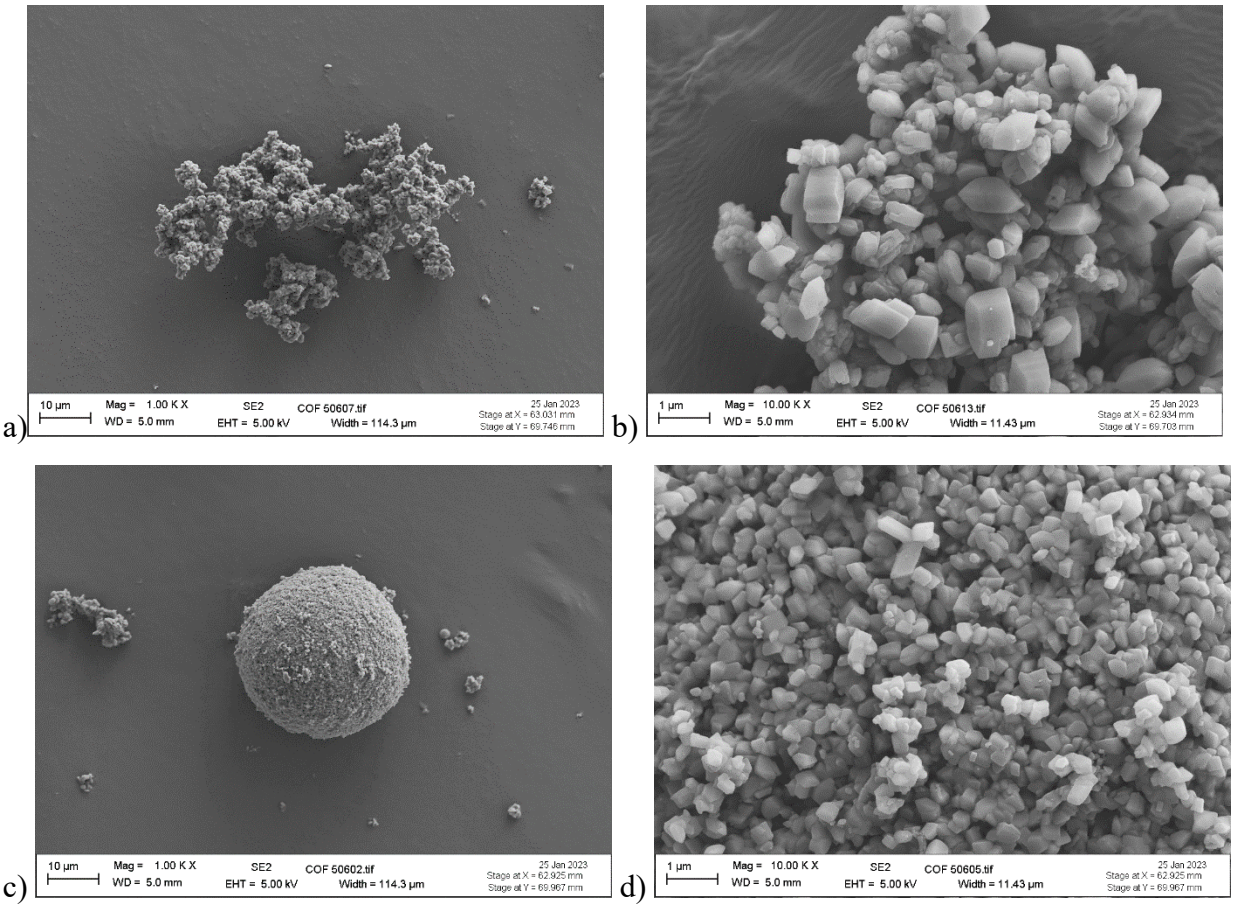

Figure 46. COF 506 before milling showing a,b) clusters and c,d) spheres composed of COF 506 primary particles ranging from 250 nm to 1um in size. Images c and d are magnified to show individual COF crystals.

Milling proved to provide the most uniform and reproducible powder which yielded generally defect free films. SEM imagery of the films showed that after milling the crystals tended to be flattened and broken. It was unclear how the damage to the crystals affected the final film properties or may have led to instability in the COF crystals in certain reaction conditions.

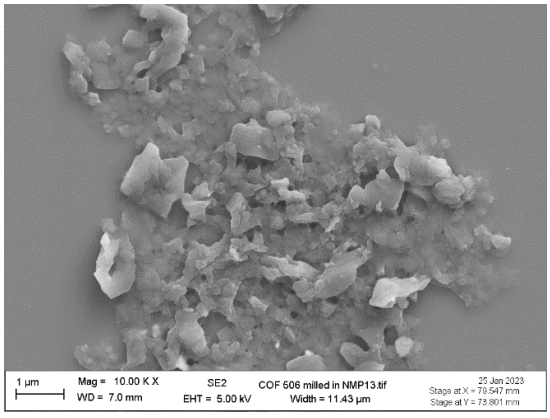

Figure 47. COF after wet-milling in NMP showing flattened and broken COF crystals.

3.7.3 Transmission FTIR analysis of PI, COF-506, and PC-COF films

Transmission IR of the polyimide, COF-506, and PI-COF composite films was performed to determine if the COF crystals were surviving the milling and polymerization processes. Figure 48 shows that the composite film has increased absorption in the 3100 to 3400 cm^{-1} and 1550 to 1700 cm^{-1} ranges which correspond well to the signature of COF 506. Additional bands at 3375, 3241, and 1669 cm-1 are consistent with N-H modes suggesting that some of the imide from the COF-506 had hydrolyzed and the resulting amines were either forming amides in the reaction or existed as free end groups. A small amount of cyanide was observable as peaks at 2151 and 2080 cm^{-1} which indicated that the washing step for this batch of COF was not fully effective in removing all the cyanide used during demetallation.

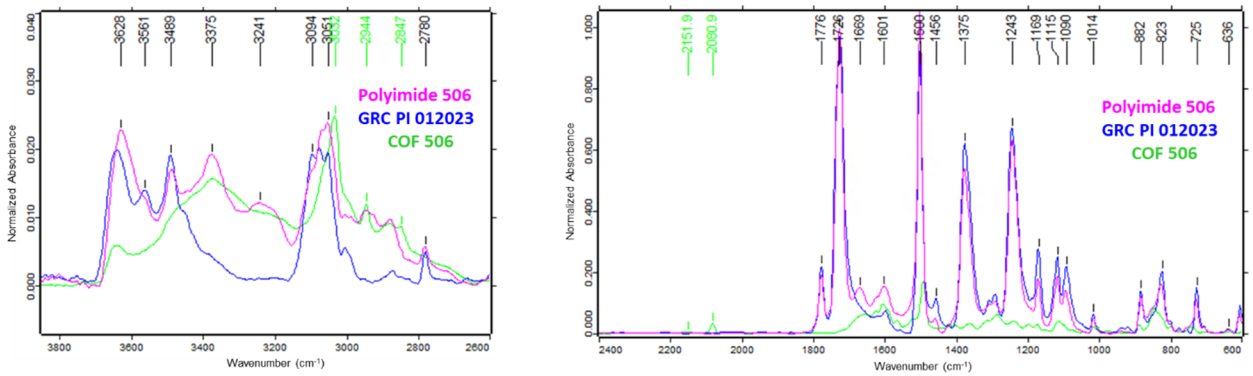

Figure 48. Transmission FT-IR of COF 506, pure polyimide (GRC PI 012023), and PI-COF composite films (Polyimide 506).

3.7.4 NMR Characterization of aromatic poly(amic acid) oligomers

To further assess the molecular weight of the matrix polyimide we submitted the poly(amic acid) pre-cursor solutions for end-group analysis by NMR. The amount of residual amine or acid end groups is inversely corelated to the molecular weight of the polymer. Approximately 2 grams of the precursor solution was pipetted onto a glass plate and placed into an oven at 75 °C for 1 hour to substantially remove the NMP solvent. We wanted to avoid complete solvent removal or temperatures which would lead to imidization, adding extra peaks into the analysis and taken too far, rendering the material insoluble in NMR solvents.

3.7.5 NMR methodology

^{1}H and 2D NMR: About 5-10mg of sample was dissolved in deuterated dimethyl sulfoxide (DMSO-D6), and ^{1}H-NMR and 2D spectra were collected on a 500 MHz Bruker Avance III spectrometer using a 5mm broadband probe. Standard experimental parameters were used including a 15s total recycle time for quantitative spectra.

^{13}C NMR: About 200 mg of sample was dissolved in 3mL DMSO with 1 wt.% $Cr(acac)_3$ relaxation agent, and ^{13}C-NMR spectra were collected on a 500MHz Bruker Avance III spectrometer using a 10mm broadband probe. Standard experimental parameters were used except

for a 5 s total recycle time for quantitative spectra. Each spectrum was collected overnight to obtain sufficient s/n.

Poly(amic acid) (PAA) is the reaction product of diamine and dianhydride in the first stage, where amide linkages are formed between the amine and anhydride, leaving a carboxylic acid group with each amide linkage formed. A further imidization reaction will close the ring to form the desired imide repeating units. Shown in **figure 49** is the structure of an aromatic PAA made from pyromellitic dianhydride (PMDA) and 4,4'-oxydiphenylamine (ODA).

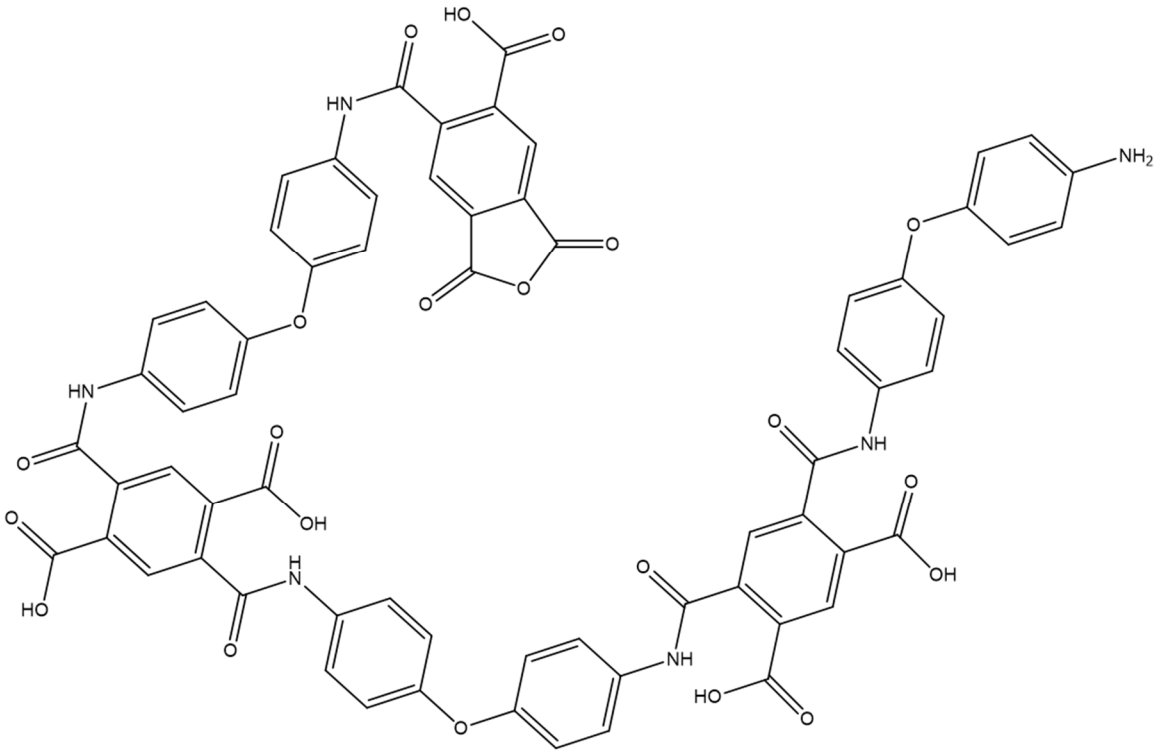

Figure 49. Structure of an aromatic PAA.

In this work, several poly(amic acid) samples were prepared in NMP solvent, and the NMP was removed from the solutions to receive yellowish to dark brown films for analysis. Shown in figure 50 is a stacked plot of the ^{1}H NMR spectra of five PAA samples with the COOH and NH peaks highlighted. The aromatic CH region is expanded in figure 51.

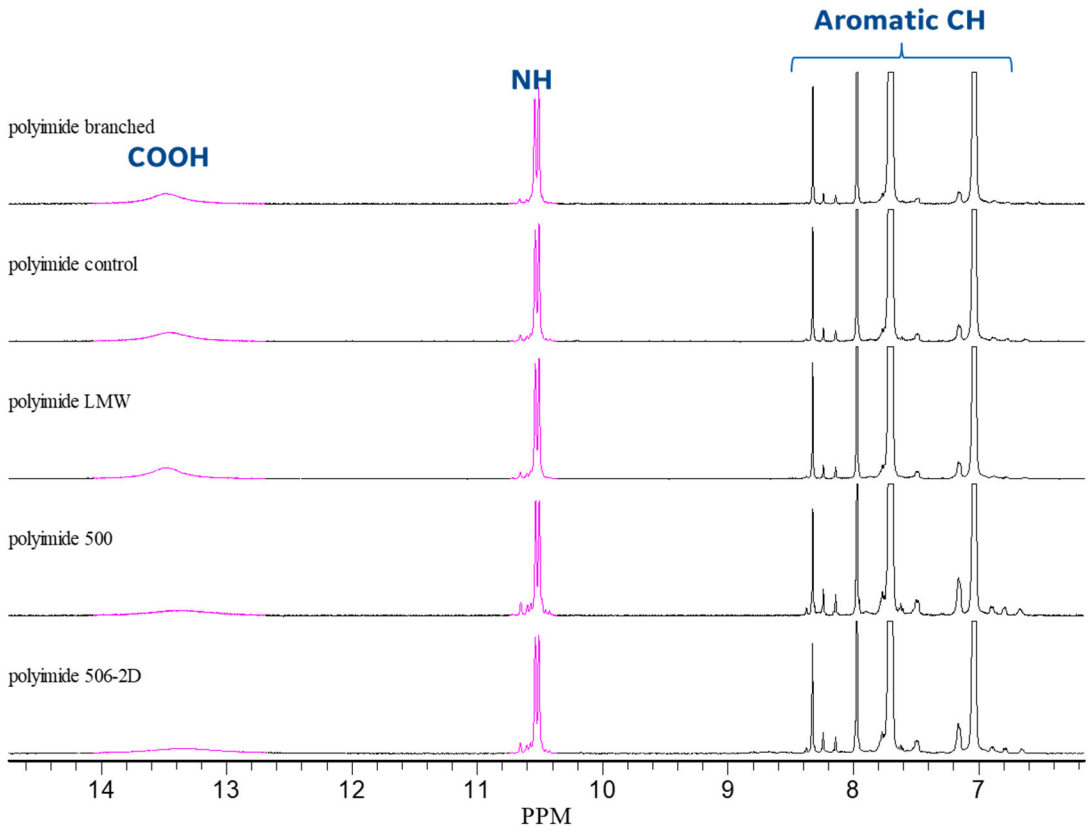

Figure 50. ^{1}H NMR spectra of PAA's in DMSO.

The amide linkage of the PAA oligomers can be formed in two isomeric conformations, cis, where the two amide linkages are on the meta positions of the PMDA ring, and trans, where the amides are on the para positions of the PDMA ring. ^{1}H NMR spectra show these isomers with some additional lower-level peaks to be assigned in further studies. The small peaks from 6.6-7.0ppm are assigned to the aromatic protons of the ODA with amine end groups according to literature reports.[21] The relative amount of the amine end groups can be calculated based on these ^{1}H NNR spectra.

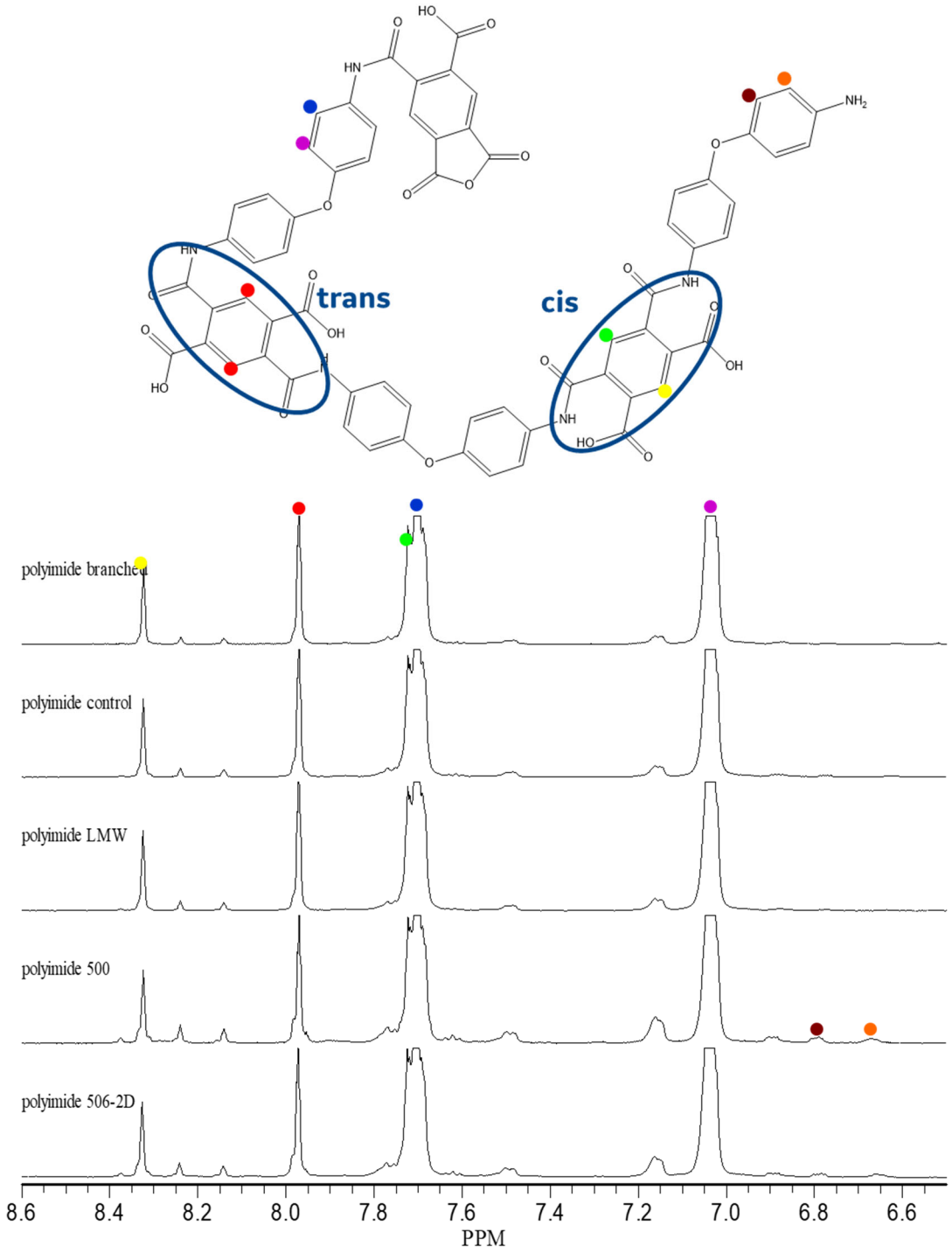

Figure 51. Structure of the cis and trans isomers of PAA repeating units (top) and 1H NMR spectra of PAA of the aromatic CH region (bottom).

Anhydride groups can be best detected using ^{13}C NMR. According to data on similar compounds in the literature, the C=O peaks of the anhydride should be in the161-163 ppm region. As shown in the ^{13}C spectra in figure 52, no anhydride can be detected in any of these five samples. Therefore, the samples appear to be rich in the amine end groups.

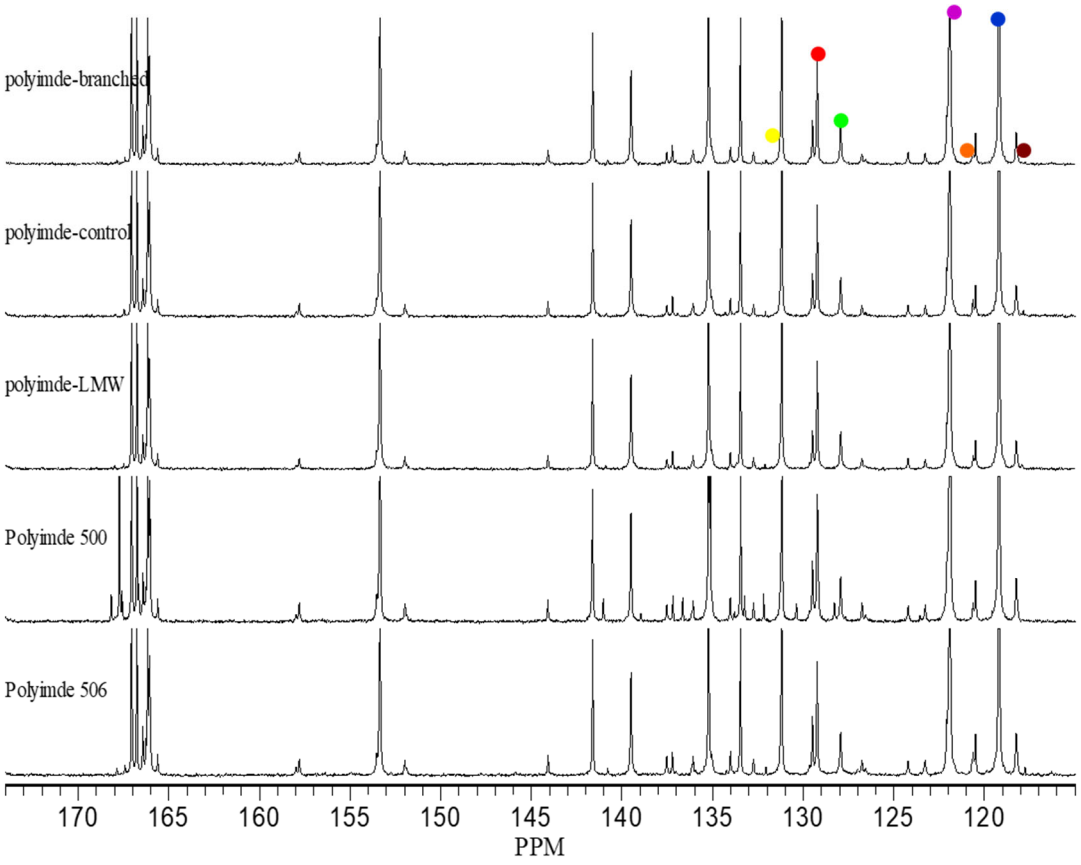

Figure 52. ^{13}C NMR spectra of PAA samples.

The amount of amine end groups relative to the amide repeating units can be calculated based on the ^{1}H spectra, as reported in table 6.

Table 6. Amount of amine end groups relative to the amide repeating units based on ^{1}H NMR.

1H-polyimde.npl	% Amine end group
polyimide branched	2%
polyimide control	2%
polyimide LMW	1%
polyimide 500	6%
polyimide 506-2D	4%

In summary, small amounts of amine end groups are detected in these PAA samples, and no anhydride is detectable. The detection limit for ^{13}C is about 0.5 mole%. The residual amine end groups found in the samples indicate that the LMW sample has the highest molecular weight and the two samples loaded with COF have significantly compromised stoichiometries. This is in good agreement with their reduced solution viscosities and mechanical strengths. The root cause of the loss of molecular weight build is unclear at this time but will need to be addressed to realize the full potential of the composite system.

3.7.6 Surface Free Energy Analysis of polymer-COF composites

Enhancements in adhesion and the improvement of specific mechanical properties in composites are achievable through the establishment of covalent chemical bonds, Coulomb forces, or acid-base interactions between the composite components. Unlike unspecific dispersion forces that act indiscriminately between solids, these mentioned force components result from precise interactions between suitable molecular groups at the interface of each partner. Consequently, in the realm of polymer surface characterization, the primary focus lies in the identification of functional groups at the surface and the characterization of their potential for interaction through the forces. In the context of describing technologically significant adhesion phenomena using physical methods and theoretical analyses, the impact of auxiliaries, impurities, and adsorbed water on adhesive strength is often overlooked. To address these so-called "third substances," we introduce the concept of "displacement forces." This concept encapsulates the capacity of these substances to diminish adhesive strength through their adsorption at the interface. It is crucial to acknowledge the competitive dynamics between adhesion and adsorption at the interface, governed by the principles of the mass action law. The extent of adhesion reduction is directly proportional to the adsorption free energy at the interface and the concentration at the interface. This concept has been previously documented in literature.

In recent research,[22] the role of interfacial adhesion between polycarbonate (PC) as a polymer and carbon fibers (CF) and glass fibers (GF) as reinforcing agents was explored using micro-Raman spectroscopy. It was effectively demonstrated that physical interactions play a pivotal role in enhancing interfacial adhesion.[22] Specifically, an indicator of the crucial π-π interaction between PC and CF was identified through the shift of the Raman band around 1604 cm^{-1}, originating from the benzene ring vibration of PC. These findings built upon earlier research on PC/carbon nanotube (CNT) composites.[23-25] Nonetheless, it is worth noting that in the previous study, the surfaces of CFs and GFs were treated with sizing and surface agents, introducing the possibility of chemical interactions influencing the interfacial properties.[22, 25] This highlights the complexity of understanding the development of interfacial adhesion between PC and reinforcing fibers.

Further adding to the complexity, research has shown that the growth of polymer crystals in proximity to CFs contributes positively to interfacial adhesion.[26, 27] Given that solution-treated PC forms a crystalline structure,[22] the role of PC crystals in enhancing interfacial properties becomes a matter of interest.

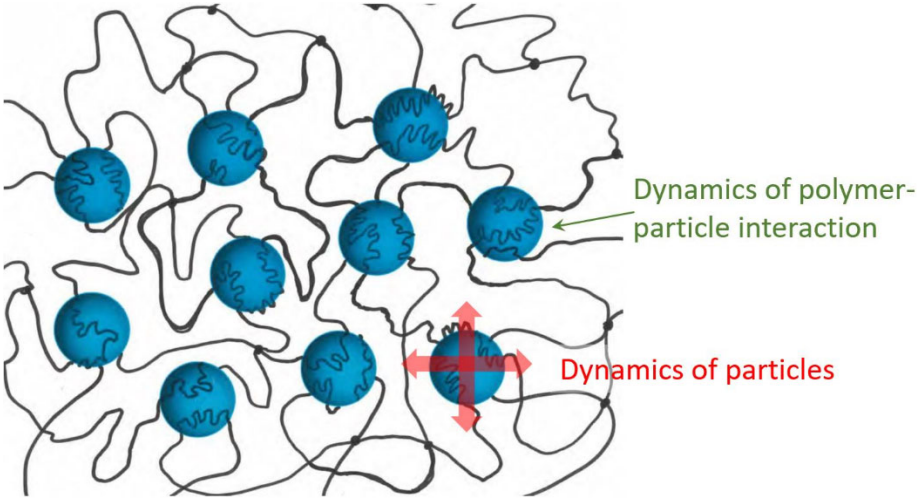

Figure 53. Molecular interactions to macroscopic behavior of polymers.

The surface free energy of a solid plays a crucial role in determining its adhesive properties. However, directly measuring the solid surface free energy can be a complex task. This is why practical procedures often rely on contact angle measurements. Advancing contact angle (ACA) data are commonly used because they are less sensitive to surface heterogeneity and roughness and allow for the calculation of surface and interfacial tension components. The solid surface free energy (γS) is determined by the combination of two components:

Equation 2

$$\gamma S = \gamma dS + \gamma pS$$

Here, γdS represents the dispersion component, and γpS is the polar component. The values of γdS and γpS for a solid can be determined using Equation 3 after measuring the contact angles (θ) of two characteristic liquids:

Equation 3

$$\gamma L1(1+\cos\theta 1) = 2(\gamma dS\gamma dL1)1/2 + 2(\gamma pS\gamma pL1)1/2$$

$$\gamma L2(1+\cos\theta 2) = 2(\gamma dS\gamma dL2)1/2 + 2(\gamma pS\gamma pL2)1/2$$

Here, γL represents the surface tension of the liquid.

For Polycarbonate, the advancing contact angles (ACAs) of Diiodomethane (DIM) and water increased as the treatment time extended, from an initial value of 30° to 36° for DIM and from 42° to 47° for water after 2 hours (Table 7). These results indicate a significant increase in the total surface free energy, from 45 to 74.2 mJ/m2 as the treatment time increased from 0 to 2 hours, which aligns with other literature findings. In addition to this, PC-COF, PDMS, PDMS-COF exhibited markedly similar trends.

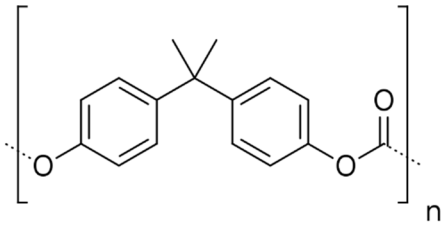

Figure 54. Molecular structure of polycarbonate.

Table 7. Surface Properties of PC films (DCE solvent).

Temp (° C)	Time (h)	rms (nm)	Contact Angle (H2O) (°)	Contact Angle (DIM) (°)	γdS	γpS	γS (mJ/m²)
23	0	1.1	42	30	30.6	14.4	45
23	0.5	4.2	43	28	27.5	18.4	45.9
23	1	1.2	45	29	27.1	51.6	78.7
23	2	2.2	47	30	19.9	54.3	74.2

For PC-COF (Table 8), the ACA of water slightly increased as the treatment time prolonged, going from 42° to 47° after 2 hours. On the other hand, the ACA of DIM decreased, moving from 61° after 0 hours to 47° after 2 hours. This suggests a significant increase in the total surface free energy, which rose from 54.0 to 60.0 mJ/m2 as the treatment time.

Table 8. Surface Properties of PC-COF films (DCE solvent).

Temp (° C)	Time (h)	rms (nm)	Contact Angle (H2O) (°)	Contact Angle (DIM) (°)	γdS	γpS	γS (mJ/m²)
23	0	3.6	42	60	36.7	17.3	54.0
23	0.5	3.2	46	54	33.0	22.1	55.1
23	1	2.8	45	50	25.0	43.0	68.0
23	2	3.0	47	47	20.0	40.0	60.0

As shown in table 9, for PDMS, the advancing contact angle (ACA) of DIM exhibited a minor increase as the treatment duration extended, transitioning from 5° to 32° after 2 hours. Conversely, the ACA of water slightly increased from 26° at 0 hours to 32o after 2 hours. This pattern points to a substantial elevation in the total surface free energy, increasing from 4.5 to 8.4 mJ/m2 as the treatment duration extended from 0 to 2 hours.

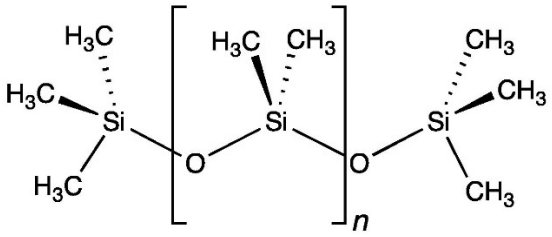

Figure 55. Molecular structure of PDMS.

Table 9. Surface Properties of PDMS films.

Temp (° C)	Time (h)	rms (nm)	Contact Angle (H2O) (°)	Contact Angle (DIM) (°)	γdS	γpS	γS (mJ/m²)
23	0	1.1	26	5	3.1	1.4	4.5
23	0.5	4.2	27	12	2.8	1.8	4.6
23	1	1.2	29	20	2.7	5.2	7.9
23	2	2.2	32	32	3.0	5.4	8.4

As shown in table 10 , for PDMS-COF, the advancing contact angle (ACA) of DIM showed an increase as the treatment duration extended, rising from 5° to 32° after 2 hours. In contrast, the ACA of water increased, going from 26° at 0 hours to 37° after 2 hours. This observation suggests a notable surge in the overall surface free energy, climbing from 9.0 to 9.9 mJ/m2 as the treatment duration extended from 0 to 2 hours.

Table 10. Surface Properties of PDMS-COF films.

Temp (° C)	Time (h)	rms (nm)	Contact Angle (H2O) (°)	Contact Angle (DIM) (°)	γdS	γpS	γS (mJ/m²)
23	0	1.1	26	5	6.1	2.9	9.0
23	0.5	4.2	30	23	5.5	3.7	9.2
23	1	1.2	33	30	5.4	7.3	12.7
23	2	2.2	37	32	6.0	3.9	9.9

Modifying the degree of intra- or intermolecular hydrogen bonding also affects the surface free energies of the polymers. Enhanced intermolecular hydrogen bonding yields an increase in surface free energy, while a reduction in intermolecular hydrogen bonding corresponds to a decrease in surface free energy. When subjected to elevated-temperature heat treatment, materials experience the disruption of hydrogen bonding, leading to the formation of differently distributed hydrogen bonds, both intra- and intermolecular, as the material rapidly cools to ambient conditions. An extension in the thermal treatment time revealed a heightened proportion of free hydroxyl groups within the material. Furthermore, an increase in the fraction of intermolecular hydrogen bonds aligned with an augmented surface free energy for the polymer after undergoing

thermal treatment. In contrast, an ABS polymer film exhibited an increase in the fraction of intermolecular hydrogen bonds with increasing thermal treatment time, leading to a higher surface free energy. A similar trend was observed for two other polymers (PC-COF, PDMS-COF), where intermolecular hydrogen bonding increased as thermal treatment time extended. Insight into the area fraction of intramolecular hydrogen bonding revealed a contrasting pattern compared to intermolecular hydrogen bonding. Specifically, an increase in the fraction of intramolecular hydrogen bonding was observed for one polymer, while the others exhibited a decrease as thermal treatment time progressed.

This study aimed to untangle the contributions of PC crystals, π-π interactions, and chemical interactions to the interfacial adhesion between PC and COF's. The influences of π-π interactions and chemical interactions were isolated through the preparation of PC and PC-COF's with varying surface free energies (different processing time). Moreover, the effect of PC crystals on interfacial adhesion was examined by evaluating the interfacial shear strength of solution-treated PC composites in filaments. The findings underscored the substantial impact of annealing temperature and time on interfacial shear strength and fracture morphology at the interface. Moreover, the presence of covalent bonds between PC chains and the surface functional groups of COFs was substantiated by the strong correlation between the calculated surface free energy and the tensile strength of the spun-coated films as shown in figure 56. Further investigation in combination with micro-Raman spectroscopy may provide valuable insights into the influence of PC crystals and the π-π interaction between PC and COFs on interfacial properties.

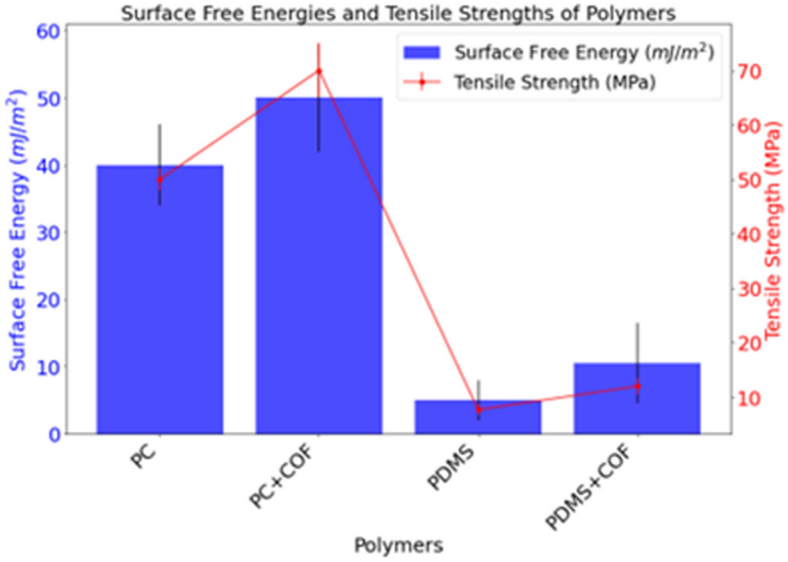

Figure 56. Relationship between the surface free energies of the polymer composites and tensile strength. (Note: The surface energies of the films are estimated at time = 0 to minimize the effect of solvent adsorption into the films)

3.7.7 ATR-FTIR analysis of PC and PC-COF films

To further understand the mechanisms driving these changes in surface free energy, we analyzed the ATR-IR spectra of the polymer films.

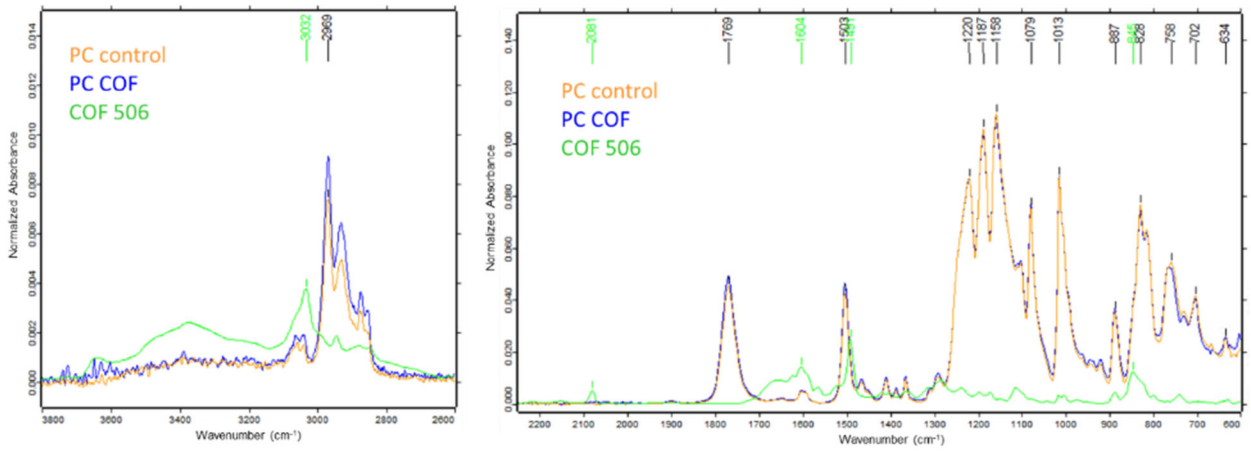

Figure 57. ATR-IR spectrographs of PC, PC-COF, and COF. Self-explanatory figure showing the individual signature of COF, which is not present in the polymer composite.

While the IR results do not show the signature of COF in the polymer composite, it gives rise to questions such as the possibility of phase separation, structured aggregation, and nm encapsulation. Further FT-IR analysis is intended to be performed on these materials to understand the system better. The extents of orientation of the chains during deformation is of considerable basic interest as well and, in the case of crystallizable elastomers, is of considerable practical importance since it leads to strain-induced crystallization and the tremendous reversible reinforcement it provides in an elastomer.

The orientation of polymer chains under strain may be conveniently described by the second Legendre polynomial:

$$\langle P2(\cos\theta)\rangle=(3\langle\cos2\theta\rangle-1)$$

where θ is the angle between the macroscopic reference axis (usually taken as the direction of strain) and the local chain axis of the polymer. The orientational behavior can be described by birefringence, directly related to the second Legendre polynomial by the expression:

$$\Delta n = [\Delta n]_0\langle P_2(\cos\theta)\rangle$$

and by the closely related technique of infrared dichroism as well. According to the theory, the birefringence is related to the strain function by the expression.

$$\Delta n = \nu kTC / V\ P(R^2 - R^{-1}) / D_1P(R^2 - R^{-1})$$

In this context, ν/V denotes the concentration of chains per unit volume, and P is a parameter that takes the value of 1 for an affine network but is adjusted to (1 - 2/φ) for a phantom network, with φ representing the junction functionality. Additionally, C is the stress-optical coefficient.

In the realm of infrared spectroscopy, the alignment of polymer chains can be assessed through the measurement of the dichroic ratio, denoted as R (R = A|/A⊥), where A| and A⊥

correspond to the absorbances of the studied infrared band when subjected to radiation polarized in parallel and perpendicular directions to the stretching axis, respectively. The orientation function is closely linked to the dichroic ratio R through the following expression.

$\langle P_2(\cos\theta)\rangle = (R+2)D_0P(R_2-R_{-1})2(3\cos 2a\text{^^}-1)(R-1)$

The angle â corresponds to the angle between the transition moment vector of the considered vibrational mode and the local chain axis within the polymer. Additionally, D0 represents the configurational factor, which has been demonstrated to be inversely correlated with the quantity of bonds (n) between two junctions. As for expressing the orientation of the transition moment vector $\langle P_2(\cos\gamma)\rangle$ relative to the direction of stretching, it can be articulated by the following expression.

A future task involves investigating to address these concerns by preparing PC-COF, PC, PDMS, and PDMS-COF systems. The objective is to achieve particle dispersions characterized as random, regular, or aggregated, with varying degrees of filler-elastomer interactions, spanning from very strong to quite weak. This forthcoming study will particularly focus on assessing the mechanical properties of these diverse filled elastomers and evaluating the levels of chain orientation under deformation through birefringence measurements and infrared spectroscopy.

3.8 Modification of Synthetic Procedures for Scaling

3.8.1 Polyimide-COF composites.

Scaling of the polyimide-COF composite was done systematically by optimizing the reaction of the polyimide in the absence of COF. Polymer films were cast from the resulting resins and the mechanical properties were measured. Additionally, film casting and imidization conditions were explored. Once a set of optimal conditions were achieved COF was added to the synthesis and results were compared to control systems of GE prepared imide and commercially available Sigma-Aldrich polyimide resin.

Table 11. Resin viscosity and film mechanical properties for polyimide resins prepared at varying monomer stoichiometries with and without COF.

	ODA	PMDA	r	viscosity (cP)	Tensile Strength	st.dev	Modulus	st.dev
GRC PI Control	1.0007	1.0919	0.9983	4380	155.5	11.9	1.2	0.08
GRC PI LMW Control	1.0001	1.0971	0.9930	9280	**164.0**		1.8	
GRC PI 500	1.0002	1.0973	0.9929	250	158.0	12.9	2.2	0.18
GRC PI 506	1.0002	1.0971	0.9931	2358	**193.6**		2.7	
F2701-128	9.9995	10.9695	0.9930	19790	161.0	20.3	1.7	0.14
F2701-129 COF 506 Amide	10.0004	10.9734	0.9927	31900	144.9	11.3	2.1	0.28
F2701-130	10.0208	11.0482	0.9880	45450	143.8	13.3	1.5	0.06
F2701-135	10.0108	10.9623	0.9947		158.2	10.5	1.5	0.04
F2701-138 COF 506 Amine	10.114	11.1002	0.9925		151.6	12.4	1.5	0.04
F2701-142	60.0205	65.8434	0.9930	236000	134.1	3.8	1.3	0.04
F2701-144	60.7552	65.8223	1.0054	14080	105.3	9.3	1.4	0.07
F2701-147 COF 506 Imine	10.0033	10.9742	0.9929	608000	119.6	8.1	1.3	0.05
F2701-147B	60.3777	65.8251	0.9991	178000	130.2	11.0	1.4	0.03
F2701-148	60.0021	66.2221	0.9870	97920	113.8	2.9	1.3	0.04

3.8.2 Experiments F2701-128, F2701-130, F2701-135: Polyimide synthesis 20-gram scale-up

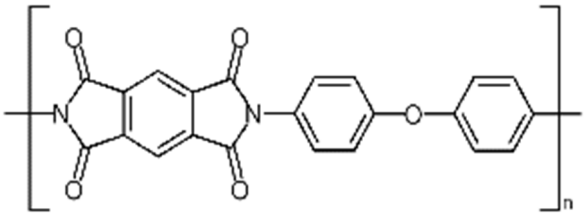

Figure 58. molecular structure of PMDA-ODA polyimide.

Three reactions were performed at the 20-gram scale at stoichiometries centered around r = 0.9930 which was found to be optimal at the 2-gram scale. The optimal ratio at this scale was found to be between r = 0.9930 and r = 0.9947. Films prepared from these resins had tensile strength of 161.0 and 158.2 MPa respectively which were within the variation of the 2-gram sample as shown in table 11.

Several synthetic optimizations were implemented at this scale which resulted in resins of improved color and viscosity.

1. A small but measurable exotherm was noted during the addition of PMDA to the room temperature ODA solution in NMP. The heating of the PMDA solution was determined to result in inferior resins in our prior update. To counteract this the ODA/NMP solution was cooled to less than 5 °C with an ice bath prior to and during the addition of the PMDA monomer. On complete addition of the monomer the reaction was heated to 75 °C for 16 hours to complete the formation of the poly(amic acid) precursors.
2. The darkened color of the resins at the 2-gram scale were reasoned to be due to oxidation of the ODA amine groups during the synthesis. Blanketing the reaction with nitrogen to eliminate air from the reaction greatly improved the color of the formed resin.

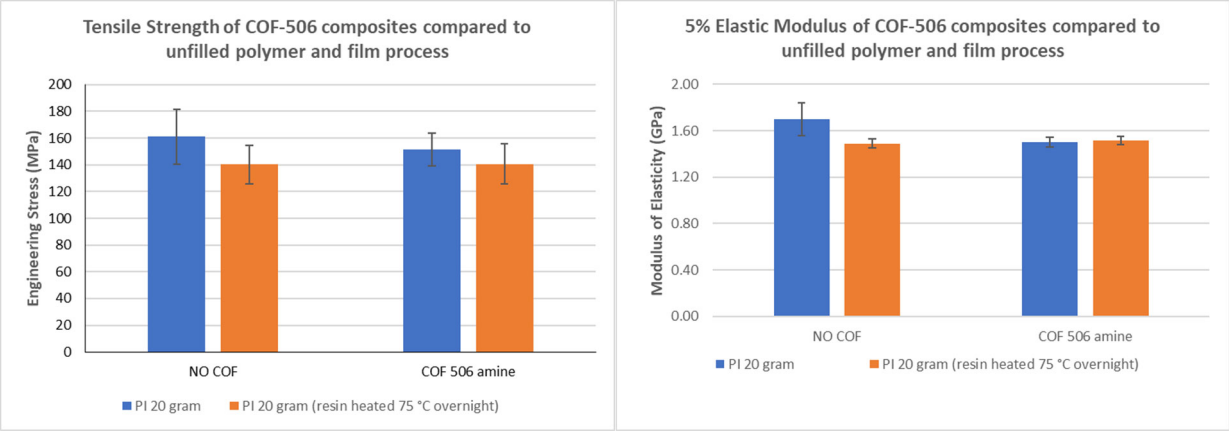

Figure 59. Reduction in a) tensile strength and b) modulus because of extended heating of the poly(imide) resin.

The standard protocol for preparing the resin included a 75 °C overnight hold to encourage complete formation of the poly(amic acid) precursors. Literature precedent suggested that on extended heating some imidization occurs producing water as a reaction by-product which can affect the viscosity and hydrolyze the poly(amic acid) precursors.[28, 29] We compared resins with and without COF before and after a 16 hour hold at 75 °C. As shown in figure 59, the films prepared after the overnight hold demonstrated a reduction in tensile strength. Only the COF free resin suffered a reduction in modulus. Based on this finding we implemented additional changes to the synthesis process. Resins prepared using this protocol tended to be significantly higher in viscosity than the resins prepared at the 2-gram scale. The control resin had a viscosity of 19790 cP at 20-gram scale versus 9280 cP at 2-gram scale.

1. After addition of the PDMA monomer the reaction is allowed to slowly warm to room temperature under nitrogen atmosphere with stirring. If the viscosity exceeds the limit of the stirring motor the stirring is stopped. The resin was allowed to equilibrate at room temperature for 16 hours before transfer to a plastic bottle.
2. Transferred resins were stored in a freezer.

3.8.3 Experiment F2701-129: Polyimide:COF 506 amide, F2701-138 Polyimide:COF 506 amine, F2701-147, and Polyimide:COF 506 imide 20-gram scale-ups.

Using the optimized conditions from the resins synthesized with no COF we prepared 3 resins at the 20-gram scale using COF-506-amine, amide, and imine. As can be seen in figure 60 and table 11, none of the COF-506 composite films showed improved tensile strength compared to the COF free film. For one set of film preparations, we also explored the effect of directly ramping to 100 °C and skipping a 75 °C overnight solvent flash step. Our prior experiments suggested that reduced time at high temperatures might benefit the mechanical properties. However, skipping the overnight flash step resulted in a loss of strength for our control, in-house control, and COF containing films.

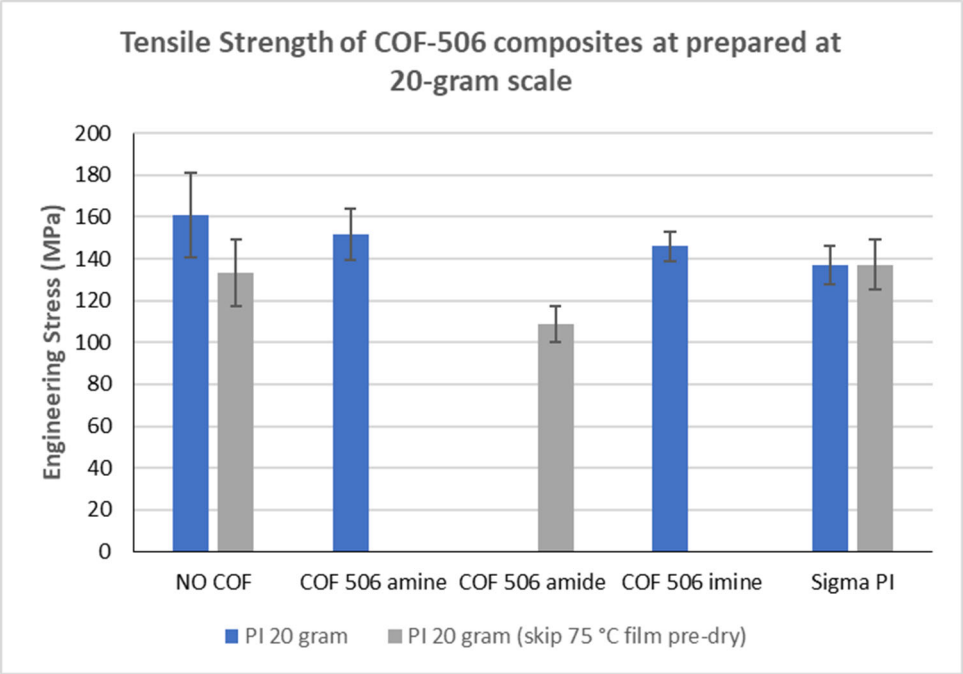

Figure 60. Tensile strength of polyimide: COF-506 composites.

3.9 Characterization of Mechanical Properties of Scaled Material

3.9.1 Experiments F2701-142, F2701-144, F2701-147B, and F2701-148 120-gram scale-ups.

After optimizing the synthesis at the 20-gram scale we proceeded to optimize the synthesis for 120-grams. This 6-fold increase in scale mimics the final scale factor where we increase to from 120 to 500-grams slightly more than a factor of 4. As before we started with a scoping of the stoichiometry space around our optimal r = 0.9930 (Table 11) to assess any drift in the process due to the shift to larger scale. Our primary concern was small losses of material as we shifted to larger transfer vessels and equipment.

At the 120-gram scale stoichiometries between r = 0.9930 and r = 0.9991 gave the highest tensile strengths; 134.1 and 130.2 MPa respectively (Table 11). We noted another significant increase in solution viscosity, up to 236,000 cP at r = 0.9930. These viscosities present mechanical issues as stirring becomes impossible with our current lab setup preventing good heat transfer in the vessel. The concentration of the solution is roughly 12 wt.% resulting in a total solution volume of slightly more than a liter necessitating a 2-L vessel.

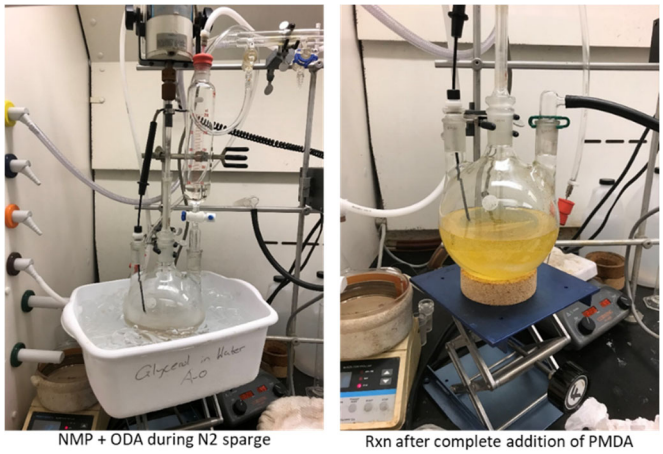

Figure 61. Reactor set-up for 120-gram scale polyimide resin synthesis.

Several optimizations were found to further improve the synthesis at this scale which may have contributed to increased viscosity. The resulting precursor films are nearly colorless prior to imidization.

1. We switched to a biosynthesis grade of NMP which is both moisture and amine free.
2. ODA is added to the flask under nitrogen flush and sealed before adding about 90% of the NMP.
3. The ODA/NMP solution is sparged with nitrogen for 1 hour while the solution is cooled to < 5 °C.
4. Addition of PMDA is done is aliquots maintaining the temperature below 10 °C.
5. All monomer residues are rinsed into the flask using the residual NMP.
6. PMDA is not fully soluble below 10 °C so once the bulk of the PMDA is in solution the cooling is removed and the reaction is allowed to warm to room temperature without external heat.

Film casting proved challenging for the high viscosity resins and our initial attempt at heating the resin yielded films of very uneven thickness. The pattern of thin spots was periodic, and we reasoned that it was due to a temperature variation on casting as the resin “unrolled” under the doctor blade. A second attempt at casting at a slower speed of 2 mm/sec with room temperature resin resulted in uniform films. We considered further diluting the resin with additional NMP, but we did not want to reduce the film thickness beyond our current 50-micron thickness.

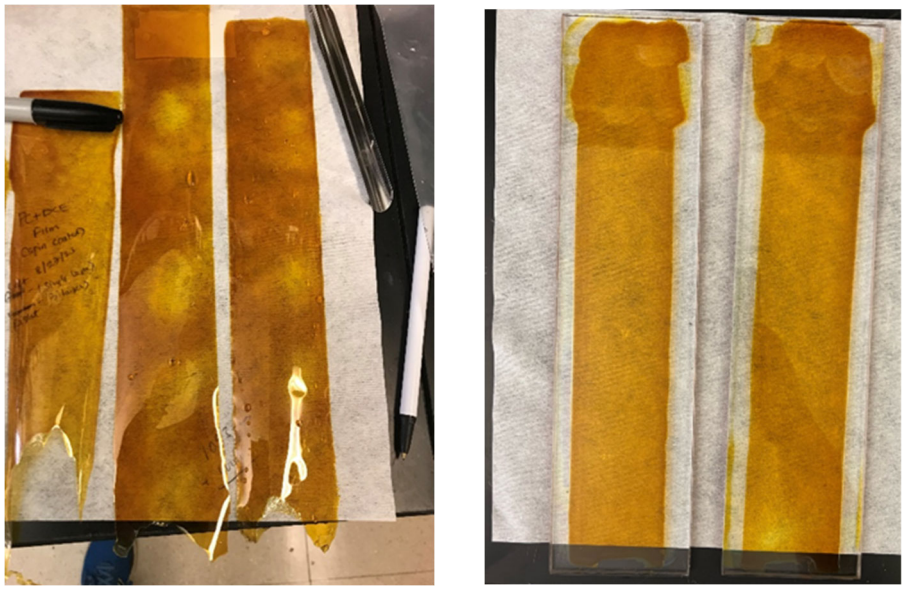

Figure 62. Films with periodic thickness variation (left) and uniform thickness (right) after imidization.

3.9.2 Rheology Characterization of the 120-gram resin batches

The surprisingly high viscosity of the 120-gram resin batches was intriguing, and we wanted to do a more in depth rheologic characterization of the resins. The viscosity of the four 120-gram batches and the most recent 20-gram composite resin with COFR 506 imine were measured using a Brookfield DVL-II Pro viscometer with the L64 spindle. The shear rate was varied from 0.5 to 100 rpm and the viscosity recorded. To assess the rheology, the data was analyzed using the Ostwald de Waele power law model using the transform from viscosity (Pa·s) to shear stress (Pa).

$$\boldsymbol{\tau = K\gamma^n}$$

n is the power law constant (unitless)
K is the flow consistency index, (Pa-s)
τ is the shear stress (Pa)

Equation 4: Ostwald de Waele power law in shear stress transform.

In all cases the power law constant, n, is close to 1 indicating Newtonian behavior with some slight deviation toward shear thickening or thinning depending on the sample. The flow consistency index, K, agrees well with the apparent viscosity and rank order of the samples (Figure 63). We were very surprised by resin F2701-147 which contained COF 506 imine as we had not seen an imine sample with such high viscosity prior. The viscosity of the undoped resins reached a maximum at r = 0.9930 in agreement with our tensile data and confirming our stoichiometry (Table 11).

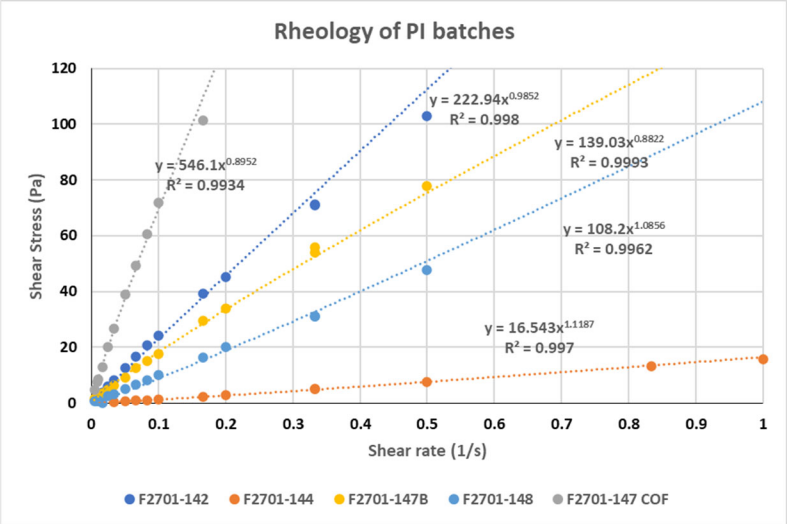

Figure 63. Ostwald de Waele power law analysis of resin viscosity.

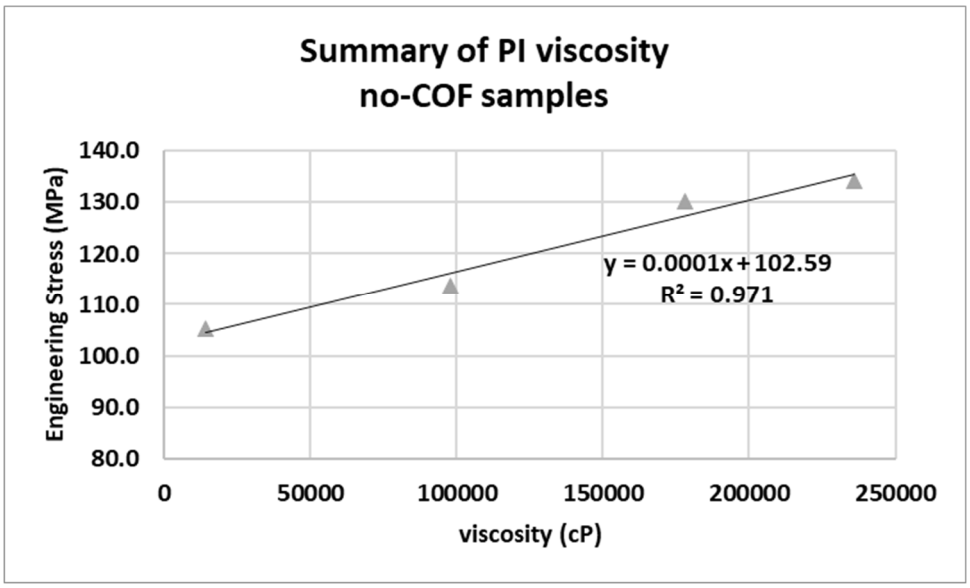

Figure 64. Correlation of resin viscosity to tensile strength for 120-gram resin batches.

3.10 Scaled-up Synthesis of Polymer-COF Composites with Improved Mechanical Properties

3.10.1 PDMS and PDMS-COF Composites (100-gram scale)

A 100-gram batch of PDMS containing 3 wt.% of COF-506-imine was prepared by milling the COF to 220 nm and blending with pre-mixed PDMS Sylgard 184 and 186 (1:1) blend for 6 h the crosslinker concentration of 10 wt.% were then added to the mixture by rigorous stirring for 2 h, the composite slurry was de-gassed in vacuum chamber prior to casting. Films were prepared by drawing casting them onto glass plates. Solvent was evaporated in a hot air oven at 70℃ for 24 h.

3.10.2 PC and PC-COF Composites (200-gram scale)

A de-gassed 200-gram batch of PC containing 3 wt.% of COF 506 imine was prepared by milling the COF to 220 nm and blending with PC in dichloroethane solvent at 10 wt.% by stirring for 24 hours. The Bi-layer films were prepared by spin casting onto glass substrates in two stages. Solvent was evaporated at room temperature overnight.

3.10.3 Material Characterization

The relationship between tensile strength and surface energy is pivotal for understanding and optimizing material performance of polymer composites. The surface energy of a polymer composite, influenced by factors such as filler type, surface modifications, and interfacial interactions, plays a crucial role in determining adhesion strength, wettability, and the effectiveness of coatings or surface treatments. A higher surface energy is often associated with enhanced adhesion and better wetting characteristics, contributing to improved interfacial interactions and stress distribution within the composite. The careful consideration of surface energy becomes particularly significant in selecting materials for composite applications, where mechanical strength is a critical parameter, hence we have estimated the surface free energy of the polymer with COF filler and with polystyrene nanoparticles as a comparative nanoparticle of similar size.

Tensile Testing

Dried films were punched out into standard ASTM D412 sample testing sizes and used for subsequent tensile testing and analysis. These punched-out samples were measured for their average thickness along their gauge length, and a pre-programmed analysis tool was employed to measure the tensile strength of these polymer composites using an Instron tester. A minor modification was made to the previously reported tensile strength testing method, which involved covering the film edges that contact the clamps in the tester with insulating 3M tape to prevent abrasion and impact resulting from the clamps' uneven surface roughness.

The tensile tests depicted in the figures offer a comprehensive view of the mechanical behavior of both neat and filled polymers, shedding light on the impact of scaling. In the neat polymer category, variations in tensile strength and elongation at break among PC and PDMS films reflect the intrinsic material characteristics. PC-COF and PDMS-COF films exhibit altered tensile strength and elongation, indicating the influence of filler incorporation. Due to constraints in material supply each scaling of the materials used a unique batch of COF and therefore the effect of scaling between 5g, 20g, and 200g batches is covariate with different batches of COF. In the comparative analysis of control samples (PC and PDMS) and those incorporating nanoparticle fillers (PC-COF, PC-PS, PDMS-COF), distinct trends in tensile strength emerge. The control samples exhibit tensile strength values of 40 MPa for PC and 8 MPa for PDMS. Introducing COF and nanoparticle fillers resulted in varied tensile strength levels, with PC-COF at different scale-ups showing 54 MPa (5g), 52 MPa (20g), and 64 MPa (200g). Similarly, PC-PS exhibits 54 MPa (5g), 55 MPa (20g), and 54 MPa (200g). For PDMS-COF, the tensile strength values are 10 MPa

(5g), 12 MPa (20g), and 18 MPa (200g). These findings highlight that there is potentially significant influence of COF processing, scale-up, or both on the tensile strength of the polymer composites. However, PC-PS, which used a single source of PS nanoparticles showed only a minor fluctuation in tensile strength across the scale-up levels, with values of 54 Mpa (5g), 55 Mpa (20g), and 54 Mpa (200g). This suggests that batch-to-batch variations in the COF nanoparticles or their processing was responsible for the varied performance on scaling. Some potential reasons include non-uniform dispersion, interfacial adhesion variations, processing condition changes, particle agglomeration, sample inhomogeneity, material consistency fluctuations, testing variability, and particle size distribution variations. To better understand the source of the variation we have characterized the test method and process development in multiple ways to better understanding the science behind the nanoparticle-matrix interphase formation and the improved mechanical properties of the films with fillers.

A)

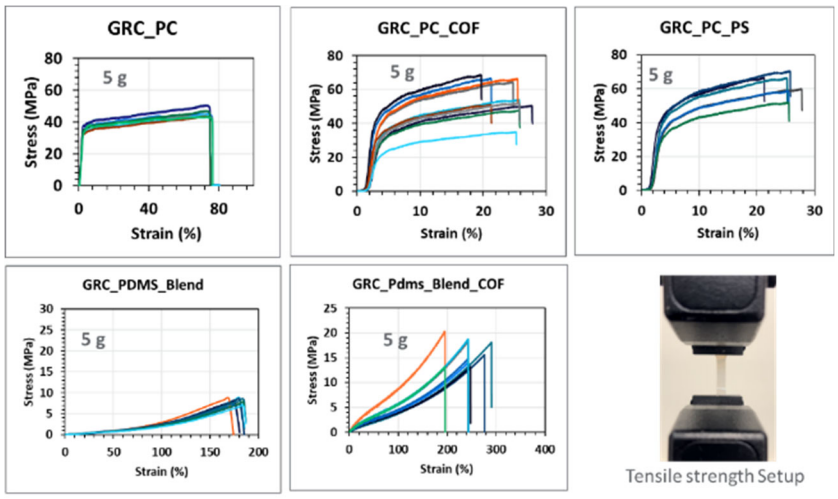

B)

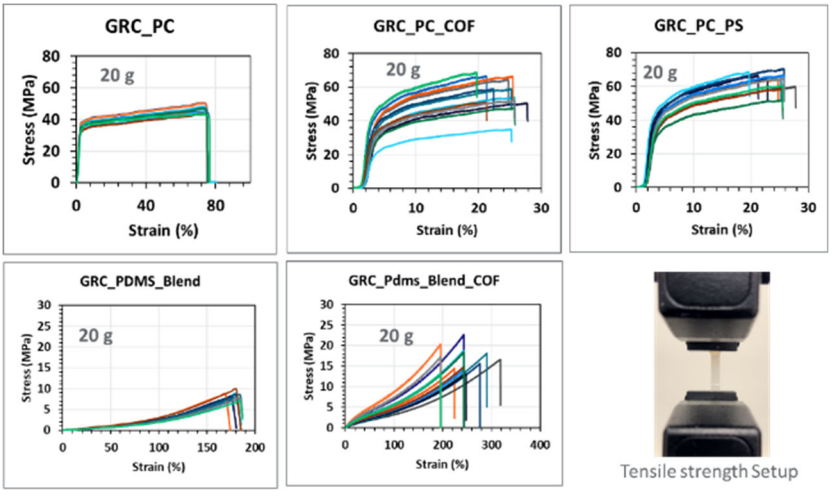

C)

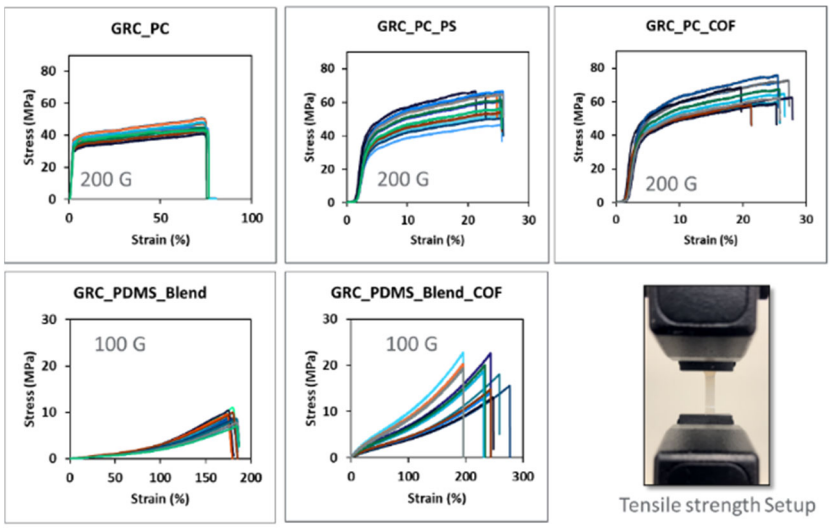

Figure 65. Tensile strength analysis of subsequent scale-up batches A) 5 g, B) 20 g and C) 200 g. Note: Higher the number of test samples, higher was the statistical significance of the data. With P value ranging from <0.12 to <0.08.

Surface Free Energy Characterization

The surface properties of PC and PDMS films were initially explored under different treatment durations while maintaining a constant temperature, as summarized in table 12. The investigation was then extended to assess the impact of different loadings of COF in PC and PDMS films, conducted in 20 g and 200 g batches. The data presented in table 12, corresponding to a treatment temperature of 23°C, illustrates changes in root mean square (rms) roughness, contact angles with water and diiodomethane (H2O and DIM), and the surface free energy components (γdS, γpS, Γs in Mj/m²) over varying treatment times while keeping the temperature constant. The thickness was measured with a micrometer tool with an accuracy of 0.01 mm on samples prepared for strength tests. Ten thickness measurements were taken for each sample. The average thickness value, along with the expanded uncertainty at a 95% confidence level and a coverage factor (k) of 2 from the normal distribution, was determined through a meticulous analysis. This comprehensive approach was applied to ten test samples for each polymer sample.